communications medicine

A Nature Portfolio journal

Article

https://doi.org/10.1038/s43856-026-01408-w

Selective blockade of latent TGF-β1 activation suppresses tissue fibrosis with good safety

Masakazu Kanamori[1,7], Izumi Sato[1,7], Christine Xing'er Koo[2,4], Yang Sun[2], Hiroki Kawauchi[1], Kenji Nakagawa[1], Atsuko Murai[3], Kentaro Asanuma[3], Siok Wan Gan[2], Chai Ling Pang[2,5], Yuichiro Shimizu[1], Meiri Shida-Kawazoe[1], Chisako Kanamaru[3], Yoko Kayukawa[1], Natsuko Hada[1], Ken Ohmine[3], Takehisa Kitazawa[1], Junichi Nezu[1,6], Tomoyuki Igawa[1] & Hideaki Shimada[1,2]

Abstract

Background Fibrosis is a hallmark of organ failure observed after chronic epithelial injury and inflammation. The transforming growth factor beta (TGF-β) is the master regulator of fibrogenesis, so blockade of the TGF-β pathway is a potential treatment strategy for fibrosis; however, the therapeutic potential of pan-TGF-β blockade is limited by side effects.

Methods We generated SOF10, a humanized antibody that targets latent TGF-β1 and selectively blocks protease- and integrin αvβ8-mediated latent TGF-β1 activation. We conducted gene expression and histological analyses in nonalcoholic steatohepatitis (NASH)/liver fibrosis and renal interstitial fibrosis models. We also evaluated the combination effect of SOF10 with an immune checkpoint inhibitor in a syngeneic mouse model and performed safety studies in mice and monkeys.

Results Here we show that SOF10 reduces fibrosis in NASH/liver fibrosis and renal interstitial fibrosis models and improves renal function in a chronic kidney disease model. Furthermore, the combination of SOF10 with an anti-PD-L1 antibody decreases tumor growth in a syngeneic mouse model. SOF10 demonstrates safety in both mice and monkeys.

Conclusions Selective blockade of latent TGF-β1 activation represents a promising approach for treating a broad range of fibrotic diseases and cancers. By specifically targeting TGF-β1, SOF10 may offer a safer and more effective therapeutic option compared to non-selective TGF-β inhibitors. This strategy has the potential to transform the treatment paradigm for fibrosis-related conditions.

Plain language summary

Fibrosis, the excessive scarring of tissues, contributes to organ failure in many diseases. While increased amounts of a protein called TGF-β can encourage development of fibrosis, complete removal of its activity causes harmful side effects. We developed a protein called SOF10 that selectively blocks only some of the activities of TGF-β1. In our studies, SOF10 reduced scarring in models of liver and kidney disease, improved kidney function, and enhanced cancer treatment when combined with immunotherapy treatments. Importantly, SOF10 proved safe in both mice and monkeys. This selective approach to blocking TGF-β1 activity could be a promising strategy for treating various fibrotic diseases and cancers with fewer side effects than complete TGF-β blockade. Our findings could lead to new treatment options for patients suffering from chronic organ damage and certain cancers.

Fibrosis refers to the pathological thickening or scarring of tissue that occurs during conditions involving chronic injury or inflammation[1]. In the long term, fibrosis leads to the functional impairment of most organs[2]. Additionally, kidney fibrosis is a common pathological feature and final manifestation of chronic kidney disease (CKD), which leads to a decline in renal function[3]. Fibrosis is also a critical risk factor for cancer, enhancing tumor cell growth, survival, migration, and drives the epithelial–mesenchymal transition[4]. In cancer patients, fibrosis can impair tumor responsiveness to immune checkpoint inhibitors (ICIs), by creating physical barriers in the tumor stroma, impeding the delivery of immunotherapeutic agents and the infiltration of immune cells into tumor tissues[5,6]. Therefore, molecular target therapy is needed to address fibrosis in affected patients.

Transforming growth factor beta (TGF-β), a cytokine with three different isoforms, TGF-β1, TGF-β2, and TGF-β3, induces fibroblast activation, which results in ECM accumulation[7]. TGF-β is thought to be a master regulator in fibrotic diseases such as, CKD, NASH, and idiopathic

[1]Research Division, Chugai Pharmaceutical Co. Ltd., Yokohama, Kanagawa, Japan. [2]Chugai Pharmabody Research Pte. Ltd., Singapore, Singapore. [3]Translational Research Division, Chugai Pharmaceutical Co. Ltd., Yokohama, Kanagawa, Japan. [4]Present address: Health Sciences Authority, Singapore, Singapore. [5]Present address: AbbVie Operations Singapore Pte. Ltd., Singapore, Singapore. [6]Present address: Mochida Pharmaceutical Co., Ltd., Gotemba, Shizuoka, Japan. [7]These authors contributed equally: Masakazu Kanamori, Izumi Sato. e-mail: shimada.hideaki12@chugai-pharm.co.jp

pulmonary fibrosis[7,8]. Moreover, TGF-β promotes cancer progression by inducing the formation of cancer-associated fibroblasts (CAFs), which leads to increased ECM production[9] and suppresses the antitumor activities of immune cells, ultimately creating an immunosuppressive environment that prevents or attenuates the efficacy of cancer immunotherapy, such as ICIs[10,11]. In addition, TGF-β is a well-characterized immunosuppressive cytokine that can modulate the functions of immune cell populations[12,13]. This suggests that TGF-β causes immunosuppressive changes in the tumor microenvironment through increased fibrosis or direct suppression of immune cells that restrain antitumor immunity.

Therefore, therapeutic approaches that block TGF-β hold great promise for the treatment of fibrosis-associated diseases and cancer.

To date, multiple agents targeting TGF-β have been developed for the treatment of fibrosis-related diseases and cancer; however, there is substantial evidence that pan-TGF blockade is not a safe treatment option. Specifically, previous nonclinical studies have shown that inhibitors of multiple TGF-β isoforms (pan-TGF-β) cause severe cardiotoxicity and bleeding[14–16]. In clinical trials, patients treated with pan-TGF-β inhibitors had a variety of toxicity-associated symptoms, such as skin neoplasms[17], bleeding and severe hemorrhagic events[18].Thus, due to the limitations of pan-TGF-β inhibition, selective inhibition of different TGF-β isoforms might be a preferred therapeutic option for such diseases.

Among the known TGF-β isoforms, TGF-β1 is the most highly expressed in the majority of solid tumors[19] and in the renal fibrosis[20], wherein the efficacy of selective antibody-mediated inhibition of TGF-β1 has been shown to be comparable in targeting all three isoforms in vivo kidney model, suggesting that TGF-β1 is the dominant TGF-β isoform driving fibrosis in the kidney[21]. Blocking the TGF-β1 pathway by selectively targeting latent TGF-β1 has been shown to enhance the antitumor immune response by inhibiting immunosuppression mediated by TGF-β1[19,22] and have an antifibrotic effect in kidney fibrosis models[23] suggesting that selectively inhibiting TGF-β1 may be a safe and effective approach. However, long-term continuous TGF-β1 blockade could increase the risk of associated toxicity, such as inflammation, limiting its clinical application for the treatment of chronic diseases. For example, in previous studies, mice with TGF-β1 deletion were reported to have a short lifespan due to inflammation in multiple organs[24,25], and TGF-β1 gene mutations that disrupt protein activity have been linked to severe infantile inflammatory bowel disease (IBD) and central nervous system diseases[24]. Together, these observations indicate that, there are several challenges related to the use of TGF-β1 blockade to mitigate fibrosis. Mature TGF-β1 is secreted in a latent complex with latency associated protein[26], called the small latent complex (SLC)[7]. While mature TGF-β1, TGF-β2, and TGF-β3 share high sequence homology, their LAP regions are quite different, allowing them to be activated in different ways[27]. Several mechanisms have been reported to elicit latent TGF-β1 activation[28–30]. Overall, there are two distinct mechanisms of latent TGF-β1 activation, protease-mediated latent TGF-β1 activation and integrin-mediated TGF-β1 activation, both of which result in the release of mature TGF-β1 from the latent complex in a tightly regulated manner. The first mechanism is mediated by proteases such as metalloproteinase (MMP) 2 and MMP9, which are highly elevated in fibrotic tissues[8,31]. Other proteases activated in fibrotic areas, such as plasmin (PLN) and plasma kallikrein (PLK), activate latent TGF-β1 by cleaving specific sites near the latency lasso of the latent complex[29].

The second mechanism of latent TGF-β1 activation is mediated by integrins and involves a conformational change induced by the binding of integrins to the RGD site of LAP[32]. Integrin-mediated latent TGF-β1 activation is associated with proper TGF-β1 function in fibrotic tissues and is critical for TGF-β-driven autoinflammation, as mice with the TGF-β1 RGE mutation and elimination of integrin-mediated activation have the same phenotype as TGF-β1 knockout (KO) mice[25]. In particular, integrins αvβ6 and αvβ8 have been reported to have the highest affinity for latent TGF-β1 among integrins and induce TGF-β1 activation[33–35]. The contribution of other αv-containing integrins, such as αvβ1, αvβ3, αvβ5, in latent TGF-β1 activation have been suggested[36,37]. However, we consider the contribution of these integrins to be minimal based on the data showing transfectants expressing αVβ6 and αVβ8, but not αV cotransfected with β1, β3, or β5 subunits, can activate pro-TGF-β[35]. Nevertheless, given that integrin β1 has been shown to be involved in mouse wound healing, we hypothesized that integrin αvβ1 may play an indirect or context-dependent role in the process of latent TGF- β 1 activation during tissue repair[38]. More critically for therapeutic development, mice that lack activity of both αvβ6 - and αvβ8-integrins develop severe autoimmunity, similar to TGF-β1 KO mice[39]. Therefore, blocking both integrin αvβ6- and αvβ8-mediated latent TGF-β1 activation is unsafe. Furthermore, integrin β6 KO mice exhibit inflammatory infiltration in the skin and increased alveolar inflammation, suggesting that αvβ6 integrin-mediated latent TGF-β1 activation is important for immune system function[39–42]. Moreover, in a clinical study of fibrosis, targeting αvβ6 with an anti-integrin αvβ6 antibody failed to result in clinical benefits and increased the likelihood of adverse events, likely reflecting on-target effects[43]. As the development of organ fibrosis therapies targeting latent TGF-β1 activation is currently lacking due to the complexity of the activation process, an improved understanding of the effects of selectively modulating of latent TGF-β1 activation is critical for the development of a safer therapeutic approach for inhibiting the TGF-β pathway in fibrosis.

In this study, given the link of integrin αvβ6 with tox events, we hypothesize that a therapeutic that would block any TGF-β1 activation, but the one mediated by integrin αvβ6 is a safe method for suppressing fibrosis. To test our hypothesis, we generated SOF10, a humanized monoclonal antibody that blocks protease- and integrin αvβ8-mediated latent TGF-β1 activation, and use it to characterize the mechanism underlying its effects. Here, we found that the selective blockade of protease- and integrin αvβ8-mediated latent TGF-β1 activation has antifibrotic effects and good safety.

Methods

Antibody generation

The anti-latent TGF-β1 antibody was first isolated from the B cells of NZW rabbits that had been immunized intradermally with a mixture of mouse and human latent TGF-β1. The anti-latent TGF-β1 antibody was humanized and further optimized by introducing multiple mutations into the heavy and light chains to improve its properties, ultimately yielding SOF10. The recombinant antibody was transfected into cells via the FreeStyle 293 Expression System or the Expi293 Expression System (Thermo Fisher Scientific). A Chinese hamster ovary (CHO) cell line was purchased and optimized at the CRO. CHO cells stably expressing SOF10 were generated at the CRO via plasmid transfection and used for large-scale production. Medium conditioned by cells expressing the antibody was purified on a column packed with Protein A resin and eluted with an acidic solution. The fractions containing the antibody were collected and subsequently subjected to gel filtration to remove high molecular weight species, if necessary. SOF10 is composed of either human or mouse IgG1 Fc with mutations to reduce Fcγ receptor binding and improve the pharmacokinetic profile[44]. The anti-pan mature TGF-β antibody GC1008 (mFc) was generated as described in US patent no. US 8,383,780 and was purified via the same method as SOF10. The anti-KLH antibody IC17 was generated as described in patent WO2019/069993 and purified via the same method as SOF10.

Protease-mediated latent TGF-β1 activation assay

hSLC was preincubated with or without antibodies or protease inhibitors for 30 min at room temperature. The preincubated latent TGF-β1 was then activated at 37 °C by the protease human plasmin (Calbiochem) for 1 h, human kallikrein (Enzyme Research Laboratories) for 2 hours or activated MMP2 or MMP9 (R&D Systems) for 2 h. The extent of TGF-β1 activation was analyzed by measuring mature TGF-β1 levels via ELISA (Human TGF-beta 1 Quantikine ELISA Kit, R&D Systems) according to the manufacturer's instructions.

Integrin αvβ6- and αvβ8-mediated TGF-β1 activation assay

HEK-Blue™ TGF-β cells were seeded into 96-well plates in assay medium (RPMI-1640 (Sigma or Nacalai Tesque) with 10% fetal bovine serum (FBS;

Sigma)). Next, SOF10, IgG1 (Sigma; #I5154, Lot: SLCK8164), an anti-TGF-β1,2,3 antibody (R&D Systems; #MAB1835-500, clone 1D11, Lot: CCI1521101, CCI1822082), an anti-αvβ8 antibody (Creative BioLabs; #HPAB-N0303-YC, clone C6D4, Lot: CB2105LX07), or an anti-integrin αVβ6 antibody (Sigma; #MAB2077Z, clone 10D5, Lot: 3916721, 3959495) was added to the wells. Next, Detroit 562 cells or LC-1sq cells were added to the wells for coincubation with HEK-Blue™ TGF-β cells overnight. Finally, the culture medium was mixed with QUANTI-Blue (InvivoGen), and the optical density at 620 nm was measured with a multilabel reader.

Cell lines

HEK-Blue™ TGF-β cells (HEK293 cell-derived TGF-β-responsive reporter cells) were purchased from InvivoGen (#hkb-tgfb) and maintained in DMEM (Sigma or Nacalai Tesque) supplemented with 10% FBS (Sigma), 1 mM sodium pyruvate (Thermo Fisher Scientific), 50 U/mL streptomycin, 50 μg/mL penicillin (Thermo Fisher Scientific) and 100 μg/mL Normocin (InvivoGen) until passage 2, after which the cells were maintained in DMEM supplemented with 10% FBS, 1 mM sodium pyruvate, 50 U/mL streptomycin, 50 μg/mL penicillin, 100 μg/mL Normocin, 30 μg/mL blasticidin (InvivoGen), 200 μg/mL HygroGold (InvivoGen) and 100 μg/mL Zeocin (InvivoGen). Detroit 562 cells were purchased from American Type Culture Collection (ATCC) (CCL-138) and maintained in EMEM (Sigma) supplemented with 10% FBS (Sigma). LC-1sq cells were purchased from Japanese Collection of Research Bioresources (JCRB) (JCRB0258) and maintained in a 1:1 mixture of RPMI-1640 (Sigma) and Ham's F12 (Thermo Fisher Scientific) supplemented with 10% FBS (Sigma). EMT6 cells were purchased from ATCC (CRL-2755) and maintained in RPMI-1640 (Sigma or Nacalai Tesque) supplemented with 10% FBS (Nichirei Biosciences or Corning). All cell lines were routinely tested for mycoplasma contamination and confirmed negative.

Analysis of binding kinetics via surface plasmon resonance

The binding kinetics between SOF10 and SLC were assessed via a Biacore™ T200 instrument (Cytiva). Anti-human Igk (BD Biosciences) was immobilized onto a sensor chip (Cytiva) by amine coupling. After SOF10 was captured on the anti-human Igk-immobilized sensor chip, hSLC, cySLC, or mSLC (Chiome Bioscience, Inc.) was injected as the analyte. Kinetic parameters were determined by fitting the sensorgrams with a 1:1 binding model using Biacore T200 Evaluation Software, version 2.0 (Cytiva). SOF10 binding to TGF-β isoforms was assessed in the same method by injecting human latent TGF-β2, 3(Chugai Pharmabody Research), human TGF-β1, 2, or 3(R&D systems) as the analyte. Analysis was carried out via Biacore T200 Evaluation Software, version 3.2.1(Cytiva).

Preparation and crystallization of the human latent TGF-β1–SOF10 Fab fragment complex

To analyze the SOF10–human latent TGF-β1 complex, the Fab fragment of SOF10 was obtained by limited digestion with the endoproteinase Lys-C (Roche), cation exchange, protein A affinity chromatography and size exclusion chromatography. A fragment of the human latent TGF-β1 protein (amino acid residues 30–390 with the C33S mutation) with a signal sequence and FLAG fused to its N-terminus was expressed in FreeStyle293F cells (Thermo Fisher Scientific) in the presence of the mannosidase I inhibitor kifunensine. Soluble human latent TGF-β1 was purified from the harvested culture supernatants by FLAG-tag affinity and size exclusion chromatography. Purified human latent TGF-β1 was mixed with the purified SOF10 Fab fragment at a molar ratio of 1:2.8 (TGF-β1: SOF10 Fab). The complex was purified by size exclusion chromatography following equilibration with 20 mM HEPES (pH 7.1) and 100 mM NaCl. The purified complexes were concentrated to approximately 12.6 mg/mL, and crystallization was carried out by sitting drop vapor diffusion at 20 °C. The reservoir solution consisted of 0.2 M sodium acetate trihydrate, 0.1 M imidazole hydrochloride (pH 8.0), and 10.0 % w/v polyethylene glycol 8,000. Crystals were cryoprotected by quickly soaking them in crystallization buffer supplemented with 20% ethylene glycol before flash cooling in liquid nitrogen.

Table 1 | X-ray data collection and refinement statistics

	human Latent TGF-β1 in complex with SOF10 fab
Data collection	
X-ray source	Swiss Light Source/X10SA
Wavelength (Å)	1.00006
Space group	*C*2
Cell dimensions *a, b, c* (Å)	225.878, 91.707, 126.120
Cell dimensions a, b, g (°)	90.000, 108.577, 90.000
Resolution (Å)	119.55 – 2.48 (2.80 – 2.48)*
R_{pim}	0.024 (0.440)*
CC(1/2)	0.999 (0.714)*
mean *I*/σ(*I*)	17.0 (1.6)*
Total observations	384791 (18778)*
Unique observations	54758 (2739)*
Completeness, spherical (%)	62.9 (10.2)*
Completeness, ellipsoidal (%)	92.1 (61.8)*
Redundancy	7.0 (6.9)*
Refinement	
Resolution (Å)	36.12 – 2.48
No. of reflections	54729
R_{work} / R_{free}[a]	28.13 / 30.98
No. atoms	8418
Protein	8302
Ligand/ion	112
Water	4
B-factors	77.44
Protein	77.11
Ligand/ion	102.52
Water	51.54
r.m.s.d. Bond lengths (Å)	0.007
r.m.s.d. Bond angles (°)	0.94
Ramachandran plot[b]	
Outliers (%)	0.66
Allowed (%)	6.55
Favored (%)	92.78
Rotamer Outliers (%)[b]	6.12

*Values in parentheses are for the highest-resolution shell.
[a]R_{free} is calculated with 5% of the reflection randomly set aside.
[b]Calculated with the program MolProbity.

Data collection and structure determination

Diffraction data were collected on the beamline X10SA at the Swiss Light Source at the Paul Scherrer Institute. After image data processing with autoPROC[45], which uses XDS[46] and AIMLESS[47] in the CCP4 software suite[48] and STARANISO[49], the initial model was solved with molecular replacement using a homology model of SOF10 Fab from MOE (Chemical Computing Group) and pro-TGF-β (PDB code: 5FFO) as the search models in Phaser[50]. The final model was refined via iterative model building in COOT[51], refinement in PHENIX[52] and BUSTER[53] and evaluation with MolProbity[54]. The collected and refined data are provided in Table 1. The structure of the complex has been deposited in the RCSB Protein Data Bank with PDB code 9VJJ. All graphical representations were prepared with PyMOL version 2.5.7 (Schrödinger, LLC).

Animal studies

All procedures associated with this study were reviewed and approved by the Institutional Animal Care and Use Committee (IACUC) in Chugai Pharmaceutical Co., Ltd., Chugai Pharmabody Research Pte. Ltd., or the Contract Research Organization. All animal studies were conducted in the animal facility accredited by the Association for Assessment and Accreditation of Laboratory Animal Care (AAALAC). Animals were housed in a temperature- and humidity-controlled room with food and water ad libitum. Sample size was determined according to our previous studies. No statistical method was used to determine sample size. The studies were not blinded.

Alport syndrome mouse model

All mice were purchased from CLEA Japan, Inc. Col4a3 KO mice are well-characterized models of Alport syndrome that exhibit progressive glomerular disease and CKD-related phenotypes, including persistent proteinuria, renal inflammation, and fibrosis. Col4a3 KO mice were generated via zinc finger nuclease (ZFN)-mediated gene editing as previously described[55]. Age-matched male WT C57BL/6 N mice with vehicle treatment were used as normal controls ($N = 4$). Male mice were used in this study to ensure more consistent disease progression and to minimize variability. The Col4a3 KO mice were divided into the following 2 groups: a group treated with an isotype control antibody IC17 (mFc) (50 mg/kg, $N = 12$) and a group treated with SOF10 (mFc) (50 mg/kg, $N = 14$). Animal grouping was conducted based on renal parameters at week 13. Since this is a spontaneous progression model, mice will be excluded from the analysis if their renal parameters are identified as outliers at the time of treatment initiation. Two mice in the isotype antibody treatment group were removed from the analysis due to severe disease progression at week 14.

All monoclonal antibodies were administered subcutaneously twice per week from 14 to 20 weeks of age, and analysis was performed at 21 weeks of age. Renal function was assessed by collecting plasma and urine every two weeks, and kidney fibrosis was evaluated at 21 weeks of age by measuring the changes in gene expression and hydroxyproline content and by histopathological analysis.

Long term CDAHFD-induced NASH/liver fibrosis mouse model

Five-week-old male C57BL/6NTac mice were purchased from Invivos Pte Ltd (Singapore) and acclimated for 1 week before the start of treatment. Male mice were used in this study to ensure more consistent disease progression and to minimize variability. The mice were divided into the following 4 groups: a group fed a normal control diet and treated with an isotype control antibody (IC17 (hFc), 30 mg/kg, $N = 5$);a group fed a CDAHFD and treated with an isotype control antibody (IC17 (hFc), 30 mg/kg, $N = 15$); and two groups fed a CDAHFD and treated with SOF10 (10 mg/kg or 30 mg/kg, $N = 15$). A choline-deficient, L-amino acid-defined, high-fat diet. The mice in the CDAHFD fed groups were given a CDAHFD (Research Diets New Brunswick, NJ, USA) for 9 weeks. The mice in the normal control group were fed with a commercial standard diet (5P75; PMI Nutrition INT'L (LabDiet), Missouri, United States). All monoclonal antibodies were administered subcutaneously once per week from when CDAHFD feeding began and up to 9 weeks. Changes in gene expression and hydroxyproline contents in the mouse livers were evaluated at week 9.

UUO-induced kidney fibrosis mouse model

Seven-week-old male C57BL/6 J mice were purchased from Jackson Laboratory Japan (Kanagawa, Japan) and acclimated for 1 week before the start of the study. Male mice were used in this study to ensure more consistent disease progression and to minimize variability. UUO was performed under isoflurane anesthesia as previously described[56]. The mice were divided into the following 5 groups: a group subjected to sham surgery and treated with an isotype control antibody (IC17 (mFc) 30 mg/kg, $N = 4$); a group subjected to UUO and treated with an isotype control antibody (IC17 (mFc) 30 mg/kg, $N = 10$); and three groups subjected to UUO and treated with SOF10 (5, 15, or 30 mg/kg, $N = 10$). All monoclonal antibodies were administered intravenously one day before surgery. Kidney fibrosis was analyzed on day 7 after UUO surgery by measuring the changes in gene expression and hydroxyproline levels in the kidneys.

Mouse EMT6 tumor model

Five- to six-week-old female specific pathogen-free (SPF) BALB/c mice were purchased from Jackson Laboratory Japan, Inc., and acclimated for 1 week before inoculation. Female mice were used in this study to maintain biological consistency, as the tumor cell line was derived from female mice. EMT6 cells in the logarithmic growth phase were harvested, washed with Hank's balanced salt solution (HBSS; Sigma), and resuspended in 50% HBSS and 50% Matrigel (Corning) at a concentration of 1×10^6 cells/mL. The mice were injected with 1×10^5 EMT6 cells (100 μL) into the left #5 mammary fat pad. When the mean tumor volume reached approximately 100–300 mm^3 (6 or 7 days after inoculation), the mice were randomized into groups on the basis of tumor volume or tumor volume and body weight. Tumor was measured with calipers and tumor volumes were calculated as $1/2 \times l \times w^2$, where l indicates length and w indicates width. The mice were treated with an isotype controls (IC17 (mFc), 10 mg/kg; rat IgG2b isotype control, BioXCell; #BE0090, clone LTF-2, Lot: 767920D1, 10 mg/kg for the first dose followed by 5 mg/kg thereafter), vehicle, anti-PD-L1 (BioXCell; #BE0101, clone 10 F.9G2, Lot: 751220D1B, 10 mg/kg for the first dose followed by 5 mg/kg thereafter), a combination of 10 mg/kg SOF10 (mFc) and anti-PD-L1 or a combination of 10 mg/kg GC1008-mFc and anti-PD-L1 antibody. The antibodies were administered 3 times per week for 2 weeks, intravenously for the first dose and intraperitoneally thereafter. The tumor volume was measured twice weekly. Mice were euthanized if they reach the humane endpoint (≥ 2000 mm^3 tumor volume, ≥20% body weight loss, or tumor necrosis and ulcerations).

Quantitative RT–PCR

Total RNA was extracted from kidney tissue via an RNeasy Mini Kit (Qiagen) and from liver tissue via QIAzol Lysis Reagent (QIAGEN). cDNA was synthesized via the use of Transcriptor Universal cDNA Master Mix (Roche Diagnostics). Quantitative PCR was performed via a TaqMan Gene Expression Assay (Thermo Fisher Scientific) on the7900HT Fast Real Time PCR System (Applied Biosystems). Mouse mitochondrial ribosomal protein L19 (*Mrpl19*: Mm00452754_m1 (FAM)) was used as the endogenous reference for kidney samples, and mouse glyceraldehyde 3-phosphate dehydrogenase (*Gapdh*: Mm99999915_g1 (FAM)) was used as the endogenous reference for liver samples. The expression of tragt genes was analyzed with the following probe sets from Applied Biosciences: *Col1a1*: Mm00801666_g1 (FAM), *Col3a1*: Mm00802300_m1 (FAM), and *Serpine1*: Mm00435858_m1 (FAM). Relative mRNA expression values were calculated by means of the double delta Ct method.

Hydroxyproline assays

Hydroxyproline assays were performed according to a previously described colorimetric method with modifications[57]. Briefly, the tissues were hydrolyzed with 6 N HCl at 95 °C overnight and cleaned by filtration. Hydroxyproline levels were measured via a hydroxyproline assay kit (BioVision) or mass spectrometry analysis.

Kidney function analysis

Plasma and urine biochemical parameters were evaluated by using a TBA-120FR autoanalyzer (Canon Medical Systems Corporation, Tochigi, Japan). Plasma and urine were collected according to the study design. Mouse blood samples were collected from the jugular vein, and urine samples were collected over 24 hours using metabolic cages. Renal function was analyzed with blood samples, collected from postcaval vein at the point of necropsy.

Histopathological analysis

Kidney tissues were fixed with 10% neutral buffered formalin solution or methanol–Carnoy's solution and then embedded in paraffin. The paraffin blocks were cut and stained with hematoxylin–eosin (HE), Sirius red, and

periodic acid–methenamine silver[58]. Digital images of Sirius red staining were used for fibrosis analysis, and PAM staining was used to analyze glomerulosclerosis. By using the Area Quantification Model v2.1.11 of HALO AI (Indica labs, New Mexico, USA, v3.3), the Sirius red-positive area was measured within the kidney area where glomeruli and original collagen fibers around arteries and the renal pelvis were excluded using a deep learning tissue classification model with DenseNet AI V2 of HALO AI. To analyze glomerulosclerosis, sclerotic and non-sclerotic glomeruli stained with PAM were annotated by a deep learning tissue classification model with DenseNet AI V2 of HALO AI. The classification model was created by a certified pathologist and confirmed by certified pathologists.

Tumor collection and CAF isolation

To analyze RNA expression in tumors, tumors were harvested 14 days after treatment initiation and placed in RNAprotect Tissue Reagent (QIAGEN). For CAF isolation, tumors were harvested 10 days after treatment initiation, minced with scissors, and dissociated via a Tumor Dissociation Kit, mouse (Miltenyi Biotec). Single cells were incubated with ACK lysing buffer (Thermo Fisher Scientific), and CAFs were isolated using a Tumor-Associated Fibroblast Isolation Kit, mouse (Miltenyi Biotec).

Analysis of RNA expression in tumors

RNA was extracted from each tumor or isolated CAFs, and gene expression was analyzed. Gene expression was assessed using the nCounter PanCancer Mouse Immune Profiling Panel (NanoString Technologies, XT-CSO-MIP1-12) for immune profiling and nCounter Mouse Fibrosis Panel v2 (NanoString Technologies, XT-CSO-MFIB2-12) for isolated CAFs, according to the manufacturer's protocol. Gene expression was digitally analyzed with the nCounter Analysis System (NanoString Technologies), and the field of view was set at 550. Normalization and data analysis were conducted with nSolver Analysis Software version 4.0 (nSolver 4.0, NanoString Technologies). Normalization of RNA loading was performed with all positive control probes and housekeeping genes included in the panel. The sample encountered QC flag or normalization flag during nSolver data processing was excluded from analysis. For pathway analysis of isolated CAFs, the pathway score was calculated by means of the nCounter Advanced Analysis version 2.0.115 (NanoString Technologies).

Flow cytometry analysis of tumor

Tumors were harvested 9 days after treatment initiation, minced with scissors, and dissociated using Tumor Dissociation Kit, mouse (Miltenyi Biotec). Single cells were incubated with ACK lysing buffer (Thermo Fisher Scientific), followed by incubated with FcR Blocking Reagent, mouse (Miltenyi Biotec) for 10 min at 4 °C. The cells were stained with following reagents: eBioscience Fixable Viability Dye eFluor 780 (Invitrogen; #65-0865-18, Lot: 2062571, 1/2000), CD45-BUV395 (BD Biosciences; #564279, clone 30-F11, Lot: 8262745, 1/100), CD3e-BUV737 (BD Biosciences; #564618, clone 145-2C11, Lot: 8236721, 1/100), CD4-BV786 (BD Biosciences; #563727, clone RM4-5, Lot: 8180556, 1/100), CD8a-PerCP-Cy5.5 (BD Biosciences; #551162, clone 53-6.7, Lot: 8243587, 1/100), CD11b- PE/Cyanine7 (BioLegend; #101216, clone M1/70, Lot: B283316, 1/100) for 30 min at 4 °C. Then, cells were fixed and permeabilized with Foxp3 / Transcription Factor Staining Buffer Set (Thermo Fisher Scientific) and incubated with Granzyme B-FITC (Biolegend; #515403, clone GB11, Lot: B282413, 1/25) for 60 min at 4 °C. The samples were analyzed with Fortessa-X20 instrument (BD Biosciences), and data analysis was performed via FlowJo v10.4.1 (FlowJo, LLC). Gating strategies for the analysis of flow cytometry data are shown in Supplementary Fig. 8.

Thirteen-week repeated intravenous dose toxicity studies of SOF10 (GLP)

Mouse study. To evaluate the toxicity of SOF10 and its systemic exposure, SOF10 was intermittently administered to ICR mice intravenously at a dose of 0 (vehicle control), 20, 60, or 200 mg/kg (volume: 3.3 mL/kg; administration speed: 1 mL/min). Both male and female mice were used in the study, and there were 16 males and 16 females in each group; specifically, 6 males and 6 females were used for the 13-week reversibility assessment, and 4 and 8 males (vehicle and SOF10 groups respectively) and 4and 8 females (vehicle and SOF10 groups respectively) were treated once every 2 weeks for 13 weeks (7 doses in total) as satellite groups for the toxicokinetic study. A total of 184 mice 92 males and 92 females that were specific pathogen free (SPF) (strain: Crl:CD1(ICR)) were aged 6 weeks at the first dose. Based on the observations during the quarantine/acclimation periods (including clinical sign, body weight, ophthalmologic examination and ADA analysis), healthy animals were selected as the candidates for test animals. Of the animals selected by the procedure described above, the animals with a favorable body weight gain (from the body weight recorded firstly during the quarantine period to that at the time of group allocation) were assigned to each group by individual body weights on the day of group allocation (5 or 4 days before the start of administration) so as to ensure uniformity of group mean body weight. This was performed by block randomization using a computer (the requisite number of groups was composed by block placement, and group numbers and animal numbers were assigned randomly). The body weight of the mice at grouping was 28.7–37.6 g among males and 21.8–29.4 g among females. The mouse study was performed at the BoZo Research Center Inc., which is accredited by AAALAC International, and was approved by the Institutional Animal Care and Use Committee of BoZo Research Center Inc.

Monkey study. To evaluate the toxicity of SOF10 and its systemic exposure, SOF10 was intermittently administered to cynomolgus monkeys intravenously at doses of 0 (vehicle control), 10, 30, or 100 mg/kg (volume: 1.7 mL/kg; administration speed: 0.34 mL/kg/min). Both male and female monkeys were used, and there were 5 males and 5 females in each group; specifically, 2 males and 2 females were used for the 13-week reversibility assessment (vehicle, 30 and 100 mg/kg), and 3 males and 3 females were given 10 mg/kg SOF10 once every 2 weeks for 13 weeks (Q2W, 7 doses in total). A total of 32 cynomolgus monkeys were used in this study (16 males and 16 females; origin: Cambodia; purpose-bred; age: 2 to 4 years old at the first dosing). Based on the observations during the quarantine/acclimation periods (including clinical sign, body weight, food consumption, ophthalmology, electrocardiography blood pressure, respiratory rate, urinalysis, hematology, blood chemistry, immunophenotyping in peripheral blood, cytokine analysis in serum and ADA analysis), healthy animals were selected as the candidates for test animals. On the final day of the acclimation period, the acclimation groups were assigned to each group by random assignment. The animals in each group were assigned animal numbers in ascending order of acclimation number. Body weight at grouping was 2.59–3.32 kg for males, and 2.57–3.24 kg for females. The cynomolgus monkey study was performed at the Shin Nippon Biomedical Laboratories, Ltd., which is accredited by AAALAC International, and was approved by the Institutional Animal Care and Use Committee of Shin Nippon Biomedical Laboratories, Ltd.

In both studies, the vehicle was 20 mmol/L L-histidine, 150 mmol/L L-arginine, 20 mmol/L L-methionine, 0.5 mg/mL polysorbate 80 and L-aspartic acid (q.s. for pH adjustment), pH 6.0. The vehicle was intermittently administered to the animals in the control group in the same manner as SOF10.

Both studies were conducted in compliance with the following GLP regulations and in accordance with the following guidelines: Good Laboratory Practice Regulations (Ministry of Health and Welfare Ordinance No. 21, March 26, 1997) and Preclinical Safety Evaluation of Biotechnology-Derived Pharmaceuticals [ICH S6 (R1)] (notification no. 0323-1, Pharmaceutical and Food Safety Bureau, Ministry of Health, Labor and Welfare, Japan, March 23, 2012).

Statistics and reproducibility

GraphPad Prism version 10 and JMP version 17 were used for statistical analysis. The data are presented as the means ± SDs unless otherwise noted.

a)

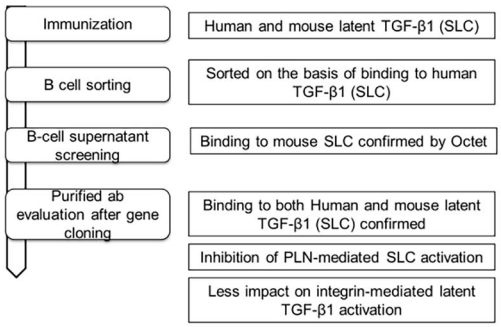

b)

Antigen	K_D ($\times 10^{-10}$ mol/L)
human latent TGF-β1	6.63 ± 0.364
cyno latent TGF-β1	7.29 ± 0.536
mouse latent TGF-β1	9.60 ± 0.968

c)

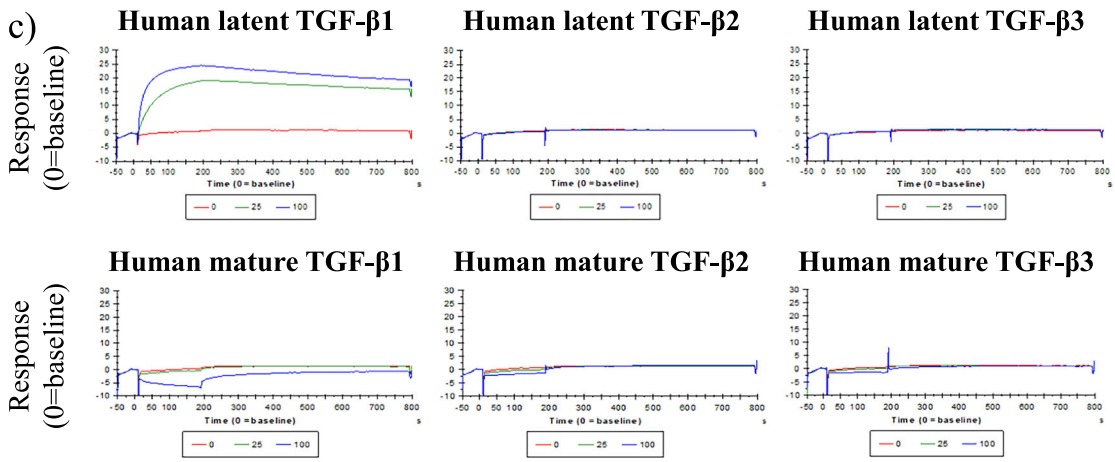

d)

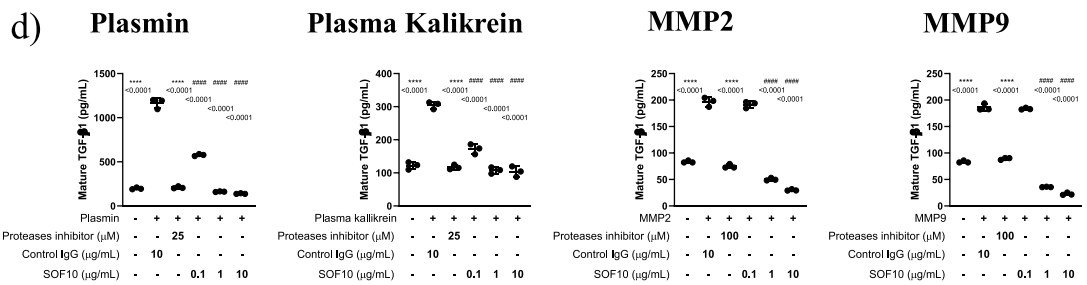

e) αvβ6-mediated TGFβ1 activation

f) αvβ8-mediated TGFβ1 activation

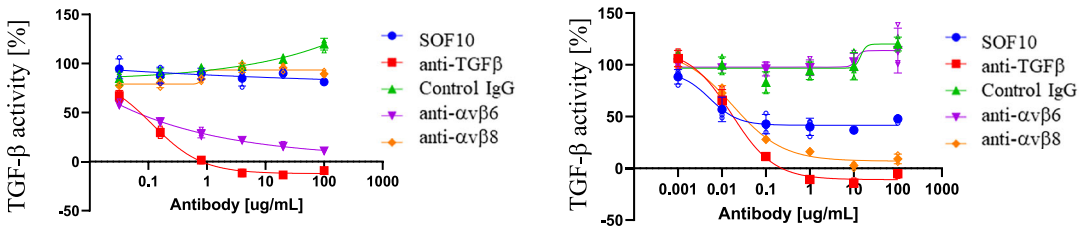

Detailed information on the statistical tests used, sample sizes(n), and *P* values, which are indicated by asterisks, are provided in each figure legend. Each experiment was independently repeated at least two times under similar conditions to confirm the reproducibility and consistency of the results.

Results

Generation and characterization of the anti-latent TGF-β1 monoclonal antibody SOF10

We began our study of whether inhibiting latent TGF-β1 activation is an effective and safe approach for treating various fibrotic diseases by

Fig. 1 | In vitro properties of the anti-latent TGF-β1 antibody SOF10. a Lead identification flow. **b** The affinities of SOF10 for latent TGF-β1 from different species were determined by surface plasmon resonance. K_D=equilibrium dissociation constant. The data in the table are presented as the mean ± standard deviation ($N = 3$). **c** The binding selectivity of SOF10 for different isoforms was determined by surface plasmon resonance. Biacore sensorgrams showing the binding of 0, 25, and 100 nM SOF10 (red, green, and blue, respectively) to human latent TGF-β1, latent TGF-β2, latent TGF-β3, mature TGF-β1, mature TGF-β2, and mature TGF-β3 are shown. **d** The inhibitory effect of SOF10 on protease-mediated latent TGF-β1 activation was evaluated via quantification of mature TGF-β1 release by ELISA. The data are reported as the means ± SDs. ***$P < 0.001$ vs. treatment with control IgG ($N = 3$). **e** Integrin αvβ6-mediated latent TGF-β1 activation was evaluated by coculturing HEK-Blue™ TGF-β reporter cells and Detroit562 cells, which endogenously express integrin αvβ6 and latent TGF-β1. TGF-β activity was measured with the SEAP reporter gene system and normalized to that observed in the absence of antibodies (considered 100%). The data are presented as the means ± SDs ($N = 3$). **f** Integrin αvβ8-mediated latent TGF-β1 activation was evaluated by coculturing HEK-Blue™ TGF-β reporter cells and LC-1 sq cells, which endogenously express integrin αvβ8 and latent TGF-β1. TGF-β activity was measured with the SEAP reporter gene system and normalized to that observed in the absence of antibodies (considered 100%). The data are presented as the means ± SDs ($N = 3$).

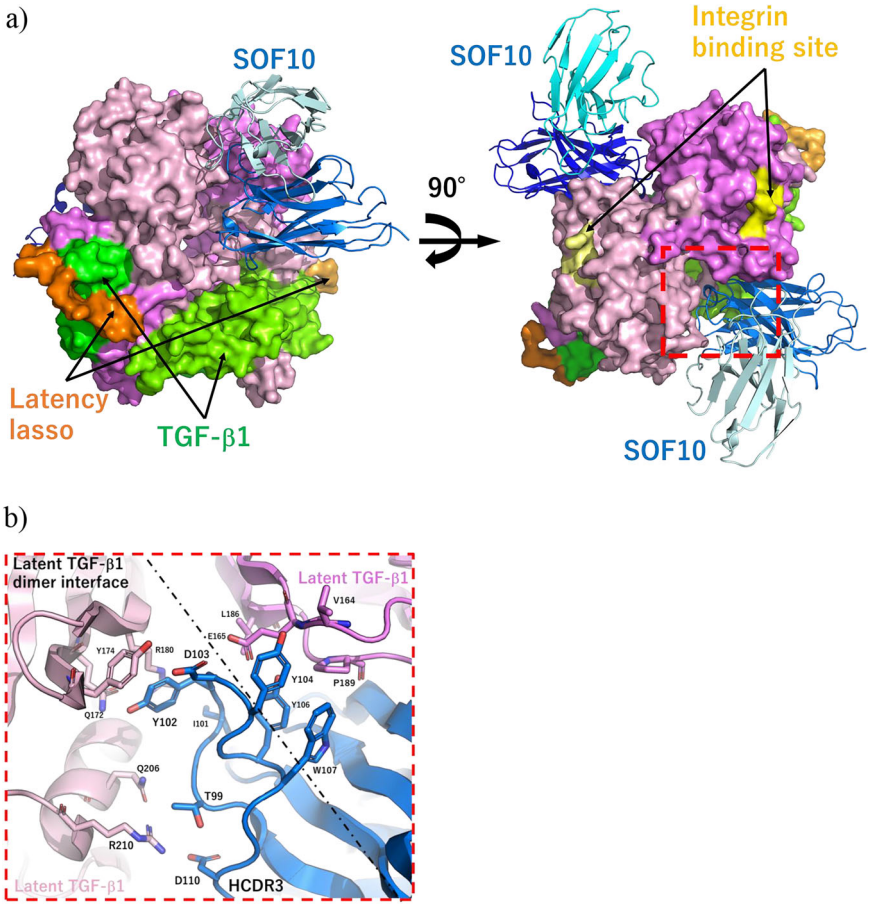

Fig. 2 | Analysis of the human latent TGF-β1–SOF10Fab complex crystal structure. a Overall structure of human latent TGF-β1 in complex with SOF10 Fab. The latent TGF-β1 dimer is shown in surface view, with the LAP domain colored light pink and violet, mature TGF-β1 colored chartreuse and green, the latency lasso colored bright orange and orange, and the integrin binding site indicated in pale yellow and yellow. The SOF10 Fab fragment is shown as a cartoon, with the heavy chain colored marine and blue, and the light chain colored pale cyan and cyan. **b** Magnified view of the interaction between the CDR3 of the heavy chain in the SOF10 Fab and the surface of the latent TGF-β1 dimer. Interacting residues are shown as sticks, with at least one atom located within 3.5 Å of either the HCDR3 of the SOF10 Fab or latent TGF-β1.

generating a humanized antibody that specifically targets latent TGF-β1, in rabbits and then optimized it. Rabbits were immunized with recombinant mouse and human SLC, and the antibodies that bound to both mouse and human latent TGF-β1 were selected. Next, we tested the chosen antibodies in both a cell-free system and a cell-based assay to identify the antibodies that can block protease-mediated latent TGF-β1 activation with less of an impact on integrin-mediated latent TGF-β1 activation (Fig. 1a). The variable regions of these antibodies were subsequently humanized and extensively engineered to improve their cross-reactivity and binding affinity. This process resulted in the generation of SOF10, which specifically binds to latent TGF-β1, but not mature TGF-β1, and has similar binding ability to human, murine, and cynomolgus monkey latent TGF-β1 (Fig. 1b, c).

To determine the effect of SOF10 on protease-mediated latent TGF-β1 activation, we tested its effects on recombinant latent TGF-β1 activation in the presence of various proteases that have been reported to activate latent TGF-β1 in cell-free systems. We mixed human latent TGF-β1 with various concentrations of SOF10 or a control antibody, and then proteases, such as PLN, PLK, MMP2, and MMP9, were added to activate human latent TGF-β1. While treatment with a protease inhibitor blocked mature TGF-β1 release from human latent TGF-β1, and compared with the control antibody, SOF10 significantly inhibited latent TGF-β1 activation by all the studied proteases in a dose-dependent manner (Fig. 1d). These data suggest that SOF10 is able to block various protease-mediated latent TGF-β1 activation.

Another well-described mechanism of latent TGF-β1 activation is integrin-mediated latent TGF-β1 activation, which most prominently involves integrins αvβ6 and αvβ8[34]. To examine integrin αvβ6-mediated latent TGF-β1 activation, we cocultured Detroit562 cells, which endogenously express integrin αvβ6, and latent TGF-β1 with HEK-Blue™ TGF-β reporter cells stably expressing TGF-β receptor 1 (TGFBRI). The results showed that the anti-integrin αvβ6 antibody inhibited TGF-β1 activation, whereas the anti-integrin αvβ8 antibody did not, indicating that TGF-β1 activation was mediated through integrin αvβ6 (Fig. 1e). Moreover, SOF10 did not affect integrin αvβ6-mediated latent TGF-β1 activation, but an anti-mature TGF-β antibody (1D11) blocked TGF-β1 signal induction (Fig. 1e). Next, to examine integrin αvβ8-mediated latent TGF-β1 activation, we cocultured LC-1 sq cells endogenously expressing integrin αvβ8 and latent TGF-β1 with HEK-Blue™ TGF-β reporter cells.

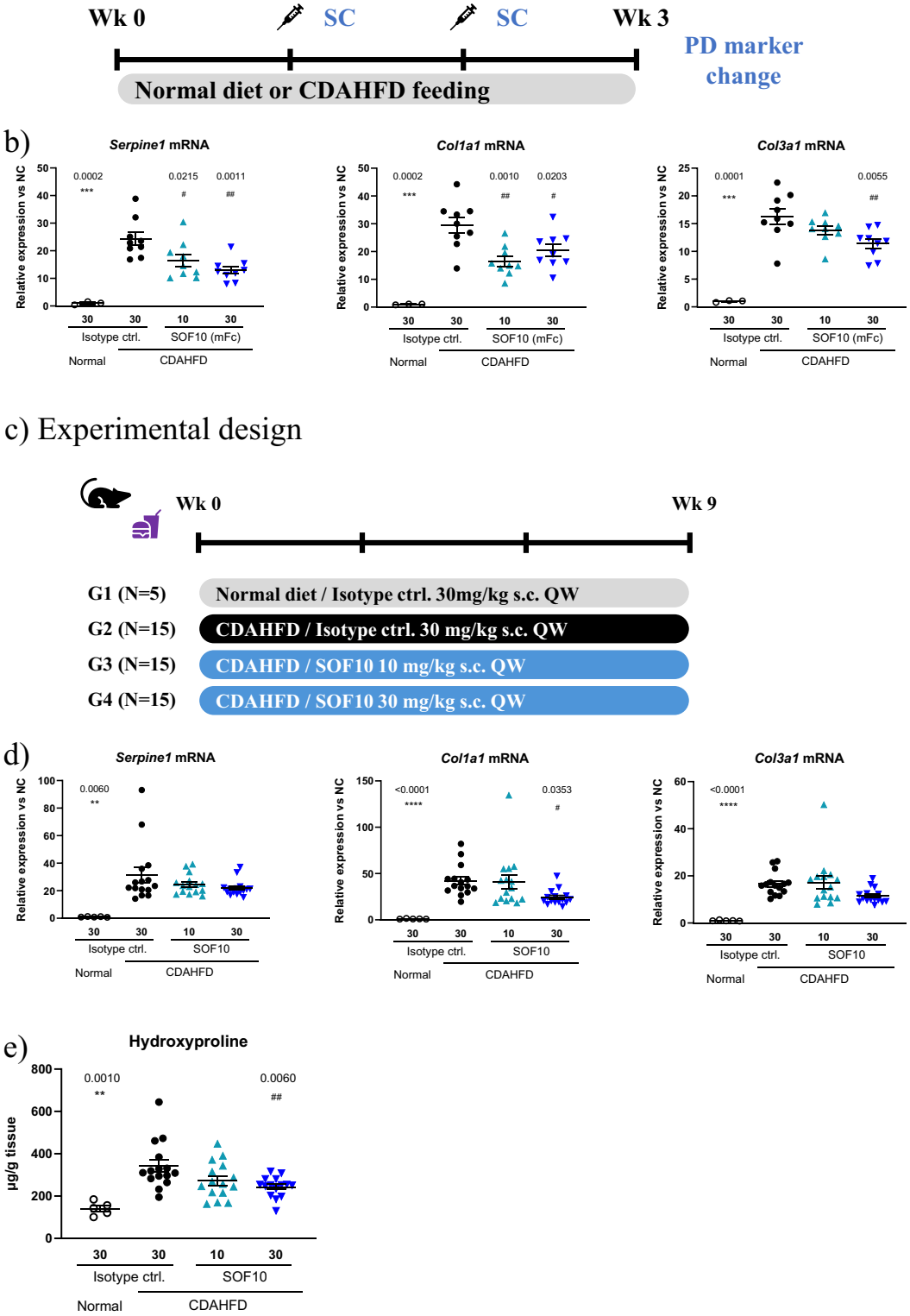

We found that the anti-integrin αvβ8 antibody inhibited TGF-β1 activation but that the anti-integrin αvβ6 antibody did not. We also found that SOF10 had a partial but dose-dependent inhibitory effect on integrin αvβ8-mediated TGF-β1 activation (Fig. 1f). Together, these results indicate the successful generation of an anti-latent TGF-β1 antibody, SOF10, that inhibits latent TGF-β1 activation driven by multiple proteases that are expressed and activated in fibrotic tissues and by integrin αvβ8 but not integrin αvβ6.

Structural analysis of SOF10

Since SOF10 was shown to inhibit latent TGF-β1 activation driven by multiple proteases and integrin αvβ8, we performed a biochemical analysis

Fig. 3 | SOF10 shows antifibrotic activity in liver fibrosis model. Liver antifibrotic activity was evaluated in both short term and long term CDAHFD-fed mice. **a** Mice fed a CDAHFD for 3 weeks to induce NASH/liver fibrosis were subcutaneously injected with either isotype control or SOF10 (mFc) once per week. **b** Antifibrotic activity was evaluated by measuring *Serpine1*, *Col1a1*, and *Col3a1* mRNA in the liver. RNA was extracted from the liver at necropsy and gene expression was analyzed by quantitative RT–PCR. $N = 3$ in the normal diet group and $N = 9$ in each the disease control and SOF10 treatment groups. **c** Mice fed a CDAHFD for 9 weeks to induce NASH/liver fibrosis were subcutaneously injected with either isotype control or SOF10 once per week. **d** Antifibrotic activity was evaluated by measuring *Serpine1*, *Col1a1*, and *Col3a1* mRNA in the liver. RNA was extracted from the liver at necropsy and gene expression was analyzed by quantitative RT–PCR. **e** Liver fibrosis was evaluated by measuring hydroxyproline levels. $N = 5$ in the normal diet group and $N = 15$ in each the disease control and SOF10 treatment groups. $^{*}P < 0.05$, $^{**}P < 0.01$, $^{***}P < 0.001$, $^{****}P < 0.0001$; ns: $P > 0.05$; unpaired two-tailed Student's t test. #$P < 0.05$, ##$P < 0.01$, ###$P < 0.001$, ####$P < 0.0001$; ns: $P > 0.05$; Dunnett's multiple comparisons test. The data are presented as the means ± SEMs.

to identify the site through which SOF10 interacts with latent TGF-β1. Specifically, we determined the structure of the SOF10 Fab fragment and latent TGF-β1 complex by X-ray crystallography. Diffraction intensity data were obtained at a resolution of 2.48 Å, and the crystallography data were obtained (Table 1). The electron density maps for CH1 and CL were ambiguous; thus, they were not built into the model. According to the crystal structure of the complex, the SOF10 Fab fragments binds to latent TGF-β1 dimers at a 2:1 ratio, with the antigen sandwiched between two SOF10 Fab fragments. The CDR loop of the SOF10 Fab fragment inserts into the dimer surface of the LAP domain of TGF-β1, as shown in Fig. 2b. The data suggested that the binding site of SOF10 does not include an integrin binding site (Fig. 2a). Interestingly, although protease-mediated TGF-β1 activation was suppressed by SOF10, this epitope of the SOF10 Fab fragment did not include a PLN/PLK digestion site near the latency lasso. Notably, we found that SOF10 inhibited the release of mature TGF-β1 mediated by PLN but did not inhibit the cleavage of the latent TGF-β1 complex by PLN (Supplementary Fig. 1). Thus, the crystallography findings might explain how mature TGF-β1 release is inhibited by SOF10 even after latent TGF-β1 cleavage.

According to a previous report[59], dimerization stabilizes latent TGF-β1. As shown in Fig. 2b and Supplementary Fig. 2, the CDR loop interacts with both sides of the latent TGF-β1 dimer, particularly the H-CDR3 loop, which plays an important role in bridging the dimer interface and enhancing the interactions between dimers. Consequently, it was inferred that SOF10 binds to the LAP dimer surface to prevent the dissociation of latent TGF-β1. We observed that the spontaneous release of mature TGF-β1 from the latent TGF-β1 complex occurred in the absence of proteases or cells, as detected by mature TGF-β1 ELISA, and that SOF10 suppressed this spontaneous release of mature TGF-β1 (Supplementary Fig. 3). This finding suggests that SOF10 enhances the interaction between LAP and mature TGF-β1 to stabilize the latent complex.

To assess the stability of SOF10 and the latent TGF-b1 complex, the melting temperatures (Tms) of the SOF10 Fab region alone, latent TGF-b1 alone, and the SOF10Fab–latent TGF-b1 complex were measured via differential scanning fluorimetry (DSF). The DSF results revealed that the Tm of the SOF10 Fab-latent TGF-β1complex was greater than that of either SOF10 or latent TGF-b1 alone. Moreover, as the temperature of the complex increased, both SOF10 and latent TGF-b1 appeared to undergo simultaneous rather than separate denaturation (Supplementary Fig. 4). Taken together, the crystallography and DSF results suggest that SOF10 stabilizes the dimeric form of latent TGF-β1 and promotes latent TGF-β1 dimerization, thus allosterically inhibiting the release of mature TGF-β1.

SOF10 inhibits liver fibrosis

Studies involving preclinical models have shown that TGF-β blockade[60], and in particular TGF-β1 inhibition[61,62], protects against organ fibrosis. Considering the ability of SOF10's to inhibit mature TGF-β1 release by stabilizing latent TGF-β1 dimers, we sought to assess whether SOF10 has an antifibrotic effects in mouse model of NASH/liver fibrosis. For this purpose, we generated a surrogate antibody, SOF10 (mFc), by replacing the Fc domain of SOF10 with the mouse Fc domain and reducing its binding to Fcγ via genetic modification. We began this set of experiments by assessing the antifibrotic effect of SOF10 (mFc) against liver fibrosis in a choline-deficient, L-amino acid-defined, high-fat diet (CDAHFD)-induced NASH/liver fibrosis mouse model, which develops progressive liver fibrosis within a short period[57]. SOF10 (mFc) was administered by injection once per week from 7 days after CDAHFD feeding. After 21 days, liver fibrosis was evaluated by measuring changes in the gene expression of the TGF-β downstream targets *Serpine1*[63] and collagen in the liver (Fig. 3a). Our analysis of TGF-β1-responsive gene expression and fibrotic markers revealed that SOF10 (mFc) decreased the expression of the *Serpine1* gene, suggesting that the TGF-β1 pathway was impacted by SOF10 (mFc) treatment. In addition, SOF10 (mFc) treatment reduced the gene expression of the major ECM components collagen type I alpha 1 (*Col1a1)* and collagen type III alpha 1 (*Col3a1)* (Fig. 3b).

We further confirmed SOF10's antifibrotic activity mice fed CDAHFD for 9 weeks. SOF10 was administered once weekly from disease induction initiation through 9 weeks (Fig. 3c). Although some markers did not reach statistical significance, SOF10 showed a trend toward suppressing TGF-β downstream targets *Serpine1*, *Col1a1*, and *Col3a1* (Fig. 3d). More importantly, liver fibrosis was evaluated by measuring hepatic hydroxyproline content (Fig. 3e). Our analysis demonstrated that SOF10 significantly reduced liver fibrosis. These results suggest that SOF10 has potential as a therapeutic option for preventing NASH/liver fibrosis.

SOF10 inhibits kidney fibrosis and improves renal function

Kidney fibrosis is considered the key underlying pathogenesis of CKD progression. To investigate whether SOF10 can ameliorate renal function by preventing renal fibrosis, we initially investigated the effect of SOF10 (mFc) on renal interstitial fibrosis using unilateral ureteral obstruction (UUO) model. This model is a surgical model commonly used to assess kidney fibrosis, particularly interstitial fibrosis, induced via tubular injury resulting from the obstruction of urine flow in the kidney[64]. SOF10 (mFc) was administered one day before UUO surgery. After 7 days, kidney fibrosis was evaluated by analyzing changes in the gene expression of TGF-β downstream target genes and by measuring the level of hydroxyproline, a widely used marker of fibrosis, in the kidney (Fig. 4a). As shown in Fig. 4b, the expression of *Serpine1* was significantly reduced by SOF10 (mFc) in the kidneys of UUO model mice. Moreover, the expression of key ECM genes involved in kidney fibrosis, namely, *Col1a1* and *Col3a1*, was also reduced by SOF10 (mFc) treatment. To evaluate kidney fibrosis at the protein level, the hydroxyproline contents in the kidney tissue was evaluated, and our results showed that hydroxyproline levels were significantly increased in the kidneys of UUO model mice but significantly reduced in the kidneys of the SOF10 (mFc) treatment groups compared with the those of the control (antibody-treated) group. These results suggest that SOF10 has the potential to reduce kidney interstitial fibrosis in multiple organs. We next asked whether attenuating fibrosis with SOF10 improves kidney function. For this analysis, we tested the effect of SOF10 (mFc) in Alport mice with collagen type IV alpha 3 (*Col4a3*) KO, which exhibits a decrease in renal function with concomitant glomerulosclerosis and interstitial fibrosis. These mice are widely used in research on Alport syndrome, which is a genetic disease characterized by the progressive loss of kidney function[65]. SOF10 (mFc) was administered by subcutaneous injections twice each week from the age of 14 weeks to 20 weeks (Fig. 4c). The ability of SOF10 (mFc) to improve renal function was assessed by comparing plasma creatinine, urea nitrogen (UN), and cystatin C (CysC) levels in the SOF10 (mFc) group to those in the isotype antibody treatment group (Fig. 4d). According to the levels of these markers, the real function was significantly improved in the SOF10 (mFc)-treated group. The improvement in renal function induced by SOF10 (mFc)

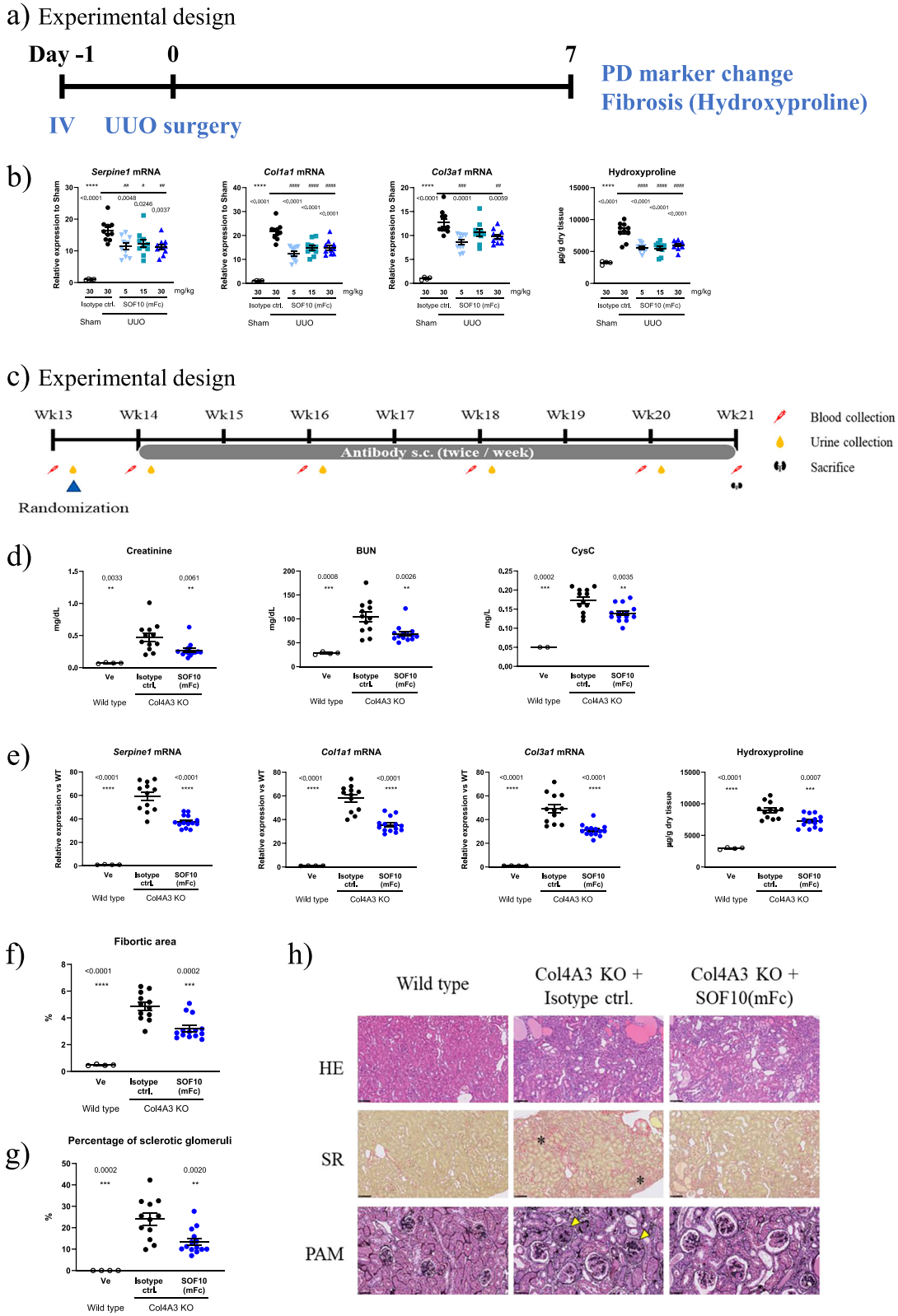

was comparable to that elicited by the pan-TGF-β antibody GC1008 (mFc) (Supplementary Fig. 5).

Next, to assess the effect of SOF10 (mFc) on TGF-β signaling and fibrosis, we evaluated change in the expression of TGF-β target genes, the level of hydroxyproline, and histopathological change in the kidney. As shown in Fig. 4e, the expression of the TGF-β downstream target *Serpine1* and the collagen genes *Col1a1* and *Col3a1* was reduced in the kidneys of Col4a3 KO mice. Additionally, the hydroxyproline content in the kidney decreased significantly in the SOF10 (mFc) treatment group compared with the isotype antibody-treated group. Since both interstitial fibrosis and glomerulosclerosis play a role in CKD progression, we examined the impact of SOF10 (mFc) on them by analyzing histopathological changes in the

Fig. 4 | SOF10 shows antifibrotic activity and ameliorates kidney function in kidney models. a, **b** Kidney antifibrotic activity was evaluated in UUO mice. **a** The mice were treated with either isotype control or SOF10 (mFc) one day before UUO surgery. **b** Antifibrotic activity was evaluated by measuring *Serpine1*, *Col1a1*, and *Col3a1* mRNA in the kidney. RNA was extracted from the kidney at necropsy and gene expression was analyzed by quantitative RT–PCR. Kidney fibrosis was evaluated by measuring hydroxyproline levels. $N = 4$ in the sham control group, $N = 10$ in the disease control group, and $N = 10$ in the SOF10 (mFc) treatment groups. $^{*}P < 0.05$, $^{**}P < 0.01$, $^{***}P < 0.001$, $^{****}P < 0.0001$; ns: $P > 0.05$; unpaired two-tailed Student's *t* test. $\#P < 0.05$, $\#\#P < 0.01$, $\#\#\#P < 0.001$, $\#\#\#\#P < 0.0001$; ns: $P > 0.05$; Dunnett's multiple comparisons test. The data are presented as the means ± SEMs. **c**–**h** Kidney fibrosis and amelioration of kidney dysfunction were evaluated in *Col4A3* KO mice. **c** The mice were subcutaneously injected with either the isotype control or SOF10 (mFc) twice a week from 14 to 20 weeks of age. **d** Kidney function was evaluated by measuring plasma creatinine, UN (BUN), and cystatin C (CysC) levels at 21 weeks of age. **e** Antifibrotic activity was evaluated by measuring *Serpine1*, *Col1a1*, and *Col3a1* mRNA and measuring hydroxyproline levels in the kidney. RNA was extracted from kidney at necropsy and gene expression was analyzed by quantitative RT–PCR. **f**–**h** Interstitial fibrosis and glomerulosclerosis were evaluated by histopathological analysis. $N = 4$ in the wild-type group, N = 12 in the disease control group and $N = 14$ in the SOF10 (mFc) treatment group. $^{*}P < 0.05$, $^{**}P < 0.01$, $^{***}P < 0.001$, $^{****}P < 0.0001$; ns: $P > 0.05$; unpaired two-tailed Student's *t* test. The data are presented as the means ± SEMs. Fibrosis areas (asterisks); glomerulosclerosis (arrowheads). HE and Sirius red staining, bar = 100 μm. PAM staining, bar = 50 μm. SR sirius red.

kidneys of Col4a3 KO mice. Consistent with the decreases in collagen gene expression and hydroxyproline content, the fibrotic area in the interstitial region was significantly reduced in the SOF10 (mFc)-treated group compared with the isotype antibody-treated Col4a3 KO mice (Fig. 4f, h). Next, we measured the percentage of sclerotic glomeruli to assess the alleviation of glomerulosclerosis. As shown in Fig. 4g, h, compared with wild-type (WT) mice, Col4a3 KO mice presented sclerotic changes in the glomeruli. Moreover, a smaller ratio of sclerotic glomeruli was observed in the SOF10 (mFc)-treated group than in the isotype antibody-treated group. Together, these data indicate that SOF10 (mFc) can reduce both renal interstitial fibrosis and glomerulosclerosis, resulting in improved renal function, in Col4a3 KO mice.

SOF10 attenuates cancer-associated fibrosis and improves the efficacy of ICI treatment

Recent studies in multiple tumor mouse models have revealed that anti-PD-L1 have greater antitumor activity when used in combination with a TGF-β neutralizing antibody than when used alone[10]. Therefore, we sought to examine the effectiveness of using SOF10 in combination with an anti-PD-L1 antibody to treat cancer. The efficacy of the combination treatment was evaluated in an orthotopic EMT6 murine breast cancer model, which exhibits an immune-excluded phenotype and expresses all TGF-β isoforms[10]. After orthotopic inoculation of EMT6 breast cancer cells, mice were treated with an isotype control, SOF10 (mFc), a pan-TGF-β antibody (GC1008 (mFc)) and/or anti-PD-L1 and tumor growth inhibition was evaluated. Consistent with a previous report[10], the combination of the pan-TGF-β antibody and anti-PD-L1 significantly inhibited tumor growth. Like the pan-TGF-β antibody, SOF10 (mFc) significantly inhibited tumor growth when used in combination with anti-PD-L1, whereas SOF10 (mFc) or anti-PD-L1 alone did not (Fig. 5a). We also evaluated the efficacy of SOF10 combined with anti-PD-L1 in a CT26 murine colorectal cancer model, in which anti-PD-L1 monotherapy has limited efficacy. Significant tumor growth inhibition was again observed after combined treatment with SOF10 (mFc) and anti-PD-L1 (Supplementary Fig. 6).

To investigate whether the combination of SOF10 and anti-PD-L1 has an effect on T-cell infiltration and activation, we harvested tumors to examine changes in the expression of genes related to CD8+ effector T cells. The expression of genes associated with CD8+ effector T cells, such as, *Ifng, Prf1, and Gzmk* was increased in the mice treated with the combination of anti-PD-L1 and SOF10 (mFc), although treatment with anti-PD-L1 or SOF10 (mFc) alone did not result in clear changes (Fig. 5b). We also found that the expression of genes related to chemokines and antigen presentation increased after combination treatment. In agreement with the change in RNA expression, flow cytometry analysis revealed that there were more CD8 + T cells and cytotoxic granzyme B + CD8 + T cells in tumors after treatment with SOF10 (mFc) and anti-PD-L1 (Fig. 5c). These results suggest that the combination of SOF10 and anti-PD-L1 can alter the immune status of tumors and lead to the influx and activation of T cells.

Previous reports have shown that TGF-β neutralization leads to alterations in CAF dynamics, greatly reducing the activity of myofibroblasts while promoting the generation of a fibroblast population characterized by a strong response to interferon (IFN), referred to as IFN-licensed CAFs (iICAFs)[66]. To evaluate the effect of SOF10 (mFc) on fibroblasts, we isolated CAFs from tumor-treated mice by magnetic cell sorting and measured the expression of fibrosis-related genes. Pathway analysis of gene expression in CAFs revealed that the expression of genes associated with the ECM synthesis and collagen biosynthesis and modification pathways decreased upon SOF10 (mFc) treatment (Fig. 5d). We also found that the expression of genes related to the type II interferon and MHC class II antigen presentation pathway was upregulated by SOF10 (mFc) and by the combination of SOF10(mFc) and anti-PD-L1, which is consistent with previous observations of the effects of anti-pan-TGF-β antibodies[66]. Taken together, these data suggest that latent TGF-β1 blockade can target CAFs by inhibiting ECM synthesis, leading to an immune-permissive environment.

The pharmacokinetics and safety profiles of SOF10 are good in both mice and monkeys

To assess the safety of SOF10, we evaluated its pharmacokinetics in cynomolgus monkeys. For this analysis, we treated monkeys with a single intravenous dose of 0.2, 1, 4, or 20 mg/kg SOF10 and measured the SOF10 plasma concentration (Supplementary Fig. 7). Although the total clearance (CL_{tot}) of SOF10 decreased with increasing dose, which is suggestive of target-mediated drug disposition, the CL_{tot} at 20 mg/kg and the volume of distribution at steady state at all doses were similar to those of typical antibodies.

Next, to support early clinical development of SOF10, toxicology studies complying with Good Laboratory Practice (GLP) were conducted; specifically, 13-week repeated intravenous dose toxicity studies in mice (20, 60, or 200 mg/kg every 2 weeks for a total of 7 doses; $N = 16$ per sex per group) and cynomolgus monkeys (10, 30, or 100 mg/kg every 2 weeks for a total of 7 doses; $N = 5$ per sex per group). In addition, SOF10 cross-reacts with latent TGF-β1 in mouse and cynomolgus monkey, and no species differences in binding affinity were observed, so both were selected as appropriate species for toxicology studies. There were no observed abnormalities (clinical signs, body weight, food consumption, ophthalmology, urinalysis, hematology, blood chemistry, myelogram, organ weight, gross pathology, or histopathology in mice; and clinical signs, general behavior and neurobehavioral function, body weight, food consumption, ophthalmology, electrocardiography, blood pressure, respiration rate, urinalysis, hematology, blood chemistry, immunophenotype, bone marrow examination, cytokine levels, necropsy, organ weight, and histopathology in cynomolgus monkeys) in either study. Overall, the no observed adverse effect level (NOAEL) was 200 mg/kg intravenously Q2W for mice and 100 mg/kg intravenously Q2W for cynomolgus monkeys, which were the highest doses tested in the two 13-week GLP studies. These results suggest that the selective inhibition of latent TGF-β1 activation by SOF10 is well tolerated in mice and monkeys and supports the use of SOF10 by patients in clinical applications.

Discussion

Fibrosis can occur in any organ due to chronic injury and inflammation, and TGF-β1 plays a central role in fibrogenesis by activating fibroblasts[67].

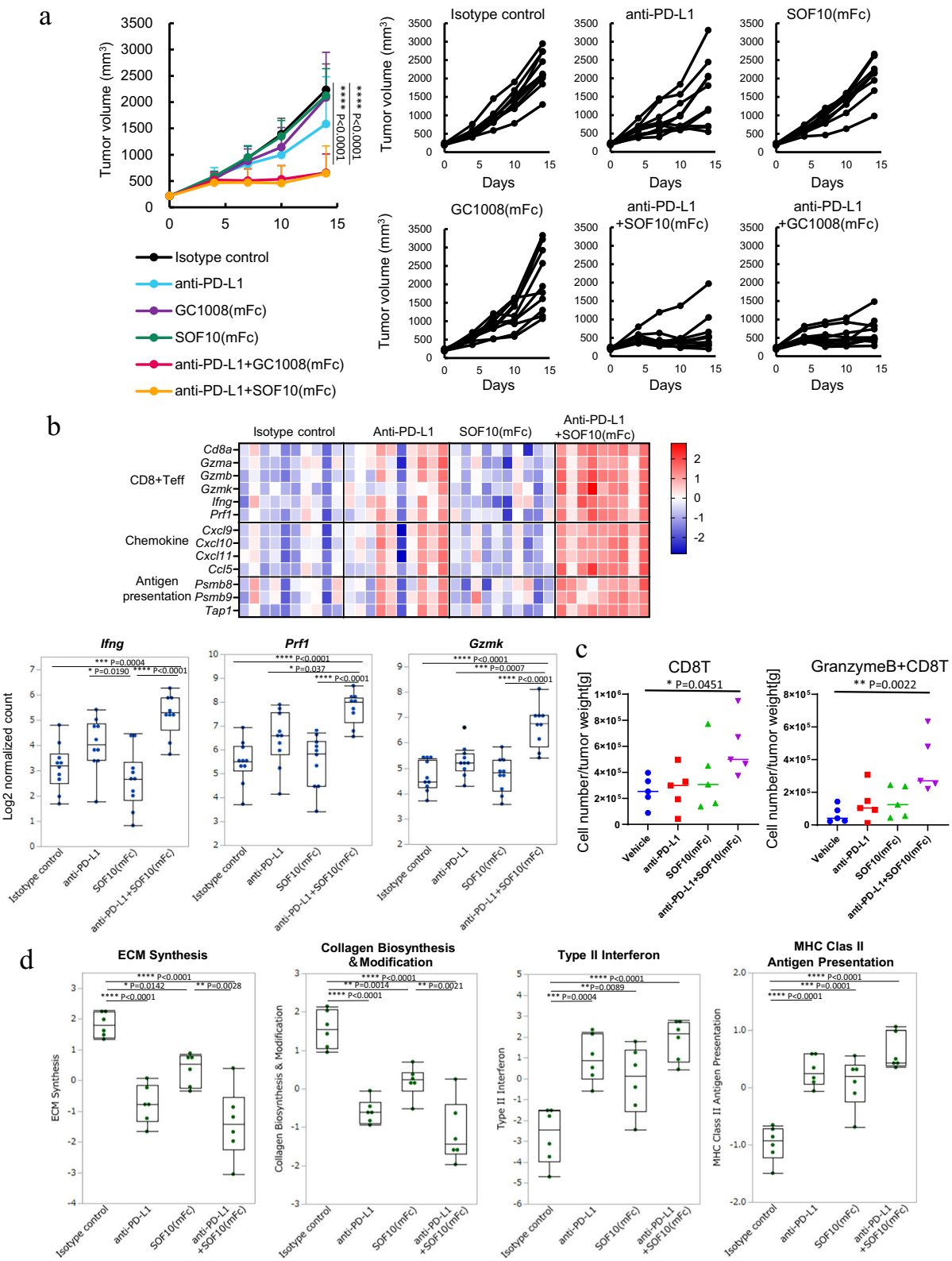

However, since long-term continuous blockade of the TGF-β signaling pathway may cause toxicity, selective blockade of TGF-β1 is the preferred therapeutic option for the treatment of fibrotic diseases. In the present study, we generated a safe antibody, SOF10, that selectively blocks protease- and integrin αvβ8-mediated latent TGF-β1 activation via a unique binding mode (Fig. 6). SOF10 inhibited fibrosis in a liver and kidney fibrosis model, improved renal function in a glomerulosclerosis model, and synergized with anti-PD-L1 by altering the fibrotic environment in cancer models. Moreover, SOF10 was well tolerated in both mice and monkeys.

In this study, we observed that SOF10 blocks key processes involved in latent TGF-β1 activation driven by proteases and integrin αvβ8. Structural analysis indicated that SOF10 binds to the upper portion of the latent TGF-β1 complex, preventing the mature TGF-β1 dissociation. This binding mode is unique and different from the previously reported antibodies

Fig. 5 | Efficacy of SOF10 (mFc) combined with an anti-PD-L1 in an EMT6 immune-excluded tumor model. a Efficacy of SOF10 (mFc) combined with anti-PD-L1 in an EMT6 mouse model. Mice with EMT6 cell-derived tumors were treated with an isotype control, SOF10 (mFc), GC1008 (mFc) and/or an anti-PD-L1 3 times per week for 2 weeks. The tumor volume was evaluated on day 14 after treatment initiation ($N = 10$). For multiple group comparisons, $^{*}P < 0.05$, $^{**}P < 0.01$, $^{***}P < 0.001$, and $^{****}P < 0.0001$ according to Dunnett test. **b** RNA expression in EMT6 tumors was measured via an nCounter Analysis System. RNA was extracted from treated tumors on day 14 after treatment initiation. The heatmap shows the normalized expression values (Z-scores) of selected genes. The boxplots show the log2 normalized counts. The center represents the median; bounds show the 25% and 75% percentiles; and whiskers extend to the most extreme data points within 1.5× the interquartile range from the quartiles. For multigroup comparisons, $^{*}P < 0.05$, $^{**}P < 0.01$, $^{***}P < 0.001$, and $^{****}P < 0.0001$ according to Tukey's test. **c** The numbers of CD8 + T cells and granzyme B + CD8 + T cells in the tumors were analyzed by flow cytometry on day 9 after treatment initiation ($N = 5$). For multi-group comparisons, $^{*}P < 0.05$, and $^{**}P < 0.01$ according to Dunnett's test. **d** Signature scores of CAFs isolated from treated tumors 10 days after treatment initiation. In box plots, the center represents the median; bounds show the 25% and 75% percentiles; and whiskers extend to the most extreme data points within 1.5× the interquartile range from the quartiles. For multigroup comparisons, $^{*}P < 0.05$, $^{**}P < 0.01$, $^{***}P < 0.001$, and $^{****}P < 0.0001$ according to Tukey's test.

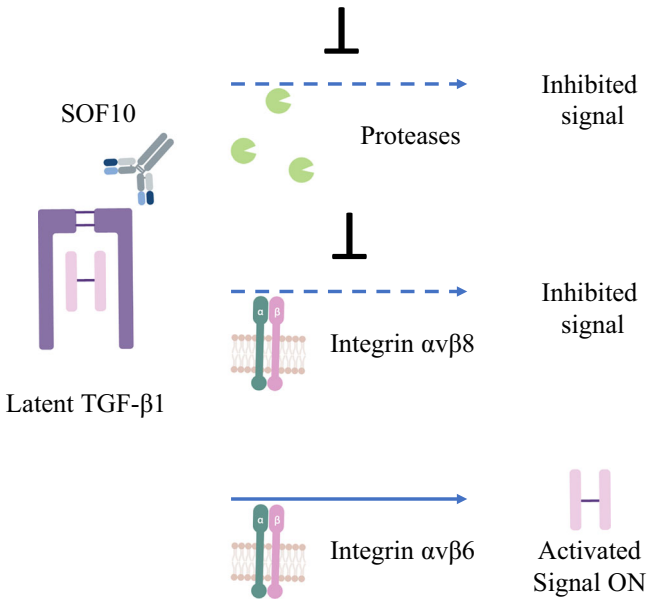

Fig. 6 | Therapeutic mechanism of SOF10. SOF10 specifically binds to latent TGF-β1, selectively inhibiting protease-mediated and integrin αvβ8-mediated activation of latent TGF-β1. SOF10 does not interfere with integrin αvβ6-mediated latent TGF-β1 activation.

targeting latent TGF-β1[19,22,23]. The binding site of SOF10 is distant from the PLK and PLN cleavage sites and the latency lasso. As shown in Supplementary Fig. 1b, although LAP cleavage by PLN cannot be inhibited by SOF10, the production of mature TGF-β1 is inhibited even after LAP cleavage. Moreover, we observed that the spontaneous release of mature TGF-β1 from the SLC occurred in the absence of proteases or cells and was suppressed by SOF10. These results suggest that the binding of SOF10 to latent TGF-β1 contributes to the stabilization of the latent complex and may prevent the dissociation of mature TGF-β1 from LAP. This idea is also supported by the DSF results (Supplementary Fig. 4).

In addition to inhibiting protease-mediated TGF-β1 activation, SOF10 inhibited TGF-β1 activation by integrin αvβ8 but not by integrin αvβ6 in our study. The binding of latent TGF-β1 to integrin avβ6 triggers a conformational change from the extended closed conformation to the extended open conformation, allowing actin cytoskeleton forces to release mature TGF-β1 from the latent complex[68]. On the other hand, integrin αvβ8-mediated TGF-β1 activation can occur without drastic conformational rearrangements and cytoskeletal forces[69]. The differential effects of SOF10 on integrin αvβ6- and αvβ8-mediated latent TGF-β1 activation might be due to differences in the tensile forces exerted by αvβ6 and αvβ8 on latent TGF-β1. It is possible that SOF10 can stabilize the latent TGF-β1 complex to prevent αvβ8-mediated activation, but not αvβ6-mediated activation accompanied by a drastic, force-mediated conformational rearrangement. Further study is needed to clarify how SOF10 inhibits the release of mature TGF-β1 from the latent complex and to characterize mechanism underlying the therapeutic effect of SOF10 in vivo under physiological conditions.

In addition to inhibiting renal interstitial fibrosis our study data suggest that inhibiting fibrosis by targeting latent TGF-β1 leads to improvements in organ function in mice. The therapeutic effect of SOF10 (mFc) was comparable to that of pan-TGF-β inhibition, suggesting that TGF-β1, but not TGF-β2 or TGF-β3, is the dominant inducer of kidney failure. These data are consistent with findings from previous studies demonstrating that TGF-β1 is the most highly expressed TGF-β isoform in kidney fibrosis and is also an upstream mediator of TGF-β2 and TGF-β3[20]. Recently, LTBP-49247, an antibody that selectively inhibits the activation of latent TGF-β1 associated with latent TGF-β-binding proteins (LTBPs) was reported to have anti-fibrotic effects in an Alport mouse model; however, its effect on renal function is not clear[23]. LTBP-49247 avoids the inhibition of GARP- and LRRC33-presented TGF-β1 activation, for sparing immune cell modulation n. However, GARP expression on ECM-producing cells, such as activated hepatic stellate cells or platelets, is involved in the development of fibrosis[70,71]. Therefore, the limited blockade of a specific SLC-LTBP complex may not have the same antifibrotic potential as the full blockade of latent TGF-β1 activation. Thus, the regulation of latent TGF-β1 activation by SOF10 is associated with GARP and LTBPs is a subsequent research topic that needs further exploration.

SOF10 was shown to inhibit tumor growth in an EMT6 murine cancer model when combined with anti-PD-L1 by modulation of the stroma cells and T cells. In cancer, fibrosis is thought to be the cause of a poor response to ICIs[5]. It has been reported that inhibiting the TGF-β pathway increases the effects of ICIs by breaking down the physical fibrotic barrier[6] and alter CAF dynamics, greatly reducing the activity of myofibroblasts[66]; however, the effect of latent TGF-β1 blockade on CAFs has not been evaluated. In this study, SOF10 (mFc) reduced the expression of genes related to ECM synthesis and collagen biosynthesis and modification in fibroblasts. We also found the infiltration and activation of T cells when SOF10 (mFc) was used in combination with anti-PD-L1. It has been reported that integrin αvβ8 expressed on tumor cells and T cells suppresses antitumor immunity by regulating TGF-β activation in immune cells[72,73]. Given that SOF10 can inhibit integrin αvβ8-mediated latent TGF-β1 activation, inhibition of immune suppression by blocking integrin αvβ8 could also contribute to the antitumor efficacy. In our study, the therapeutic effect of SOF10 (mFc) was comparable to that of pan-TGF-β inhibition, suggesting that inhibiting TGF-β1 alone is sufficient to exert antitumor effects. Although the ability of SOF10 to reduce fibrosis and inhibit immune suppression needs to be tested in more cancer models, these studies show that the combination of SOF10 and ICIs have the potential to produce synergistic anticancer effects by alleviating cancer-associated fibrosis and enhancing immune cell functions.

Selective blockade of latent TGF-β1 activation by SOF10 was well tolerated, as SOF10 did not show major toxicity in mouse or monkey toxicity studies. Inhibitors of multiple TGF-β isoforms have been shown to cause severe cardiotoxicity and bleeding in nonclinical studies[14,16]. Mouse and human genetic data suggest that some of the toxic effects of these inhibitors, including their cardiotoxicity, may be related to the inhibition of TGF-β2 and TGF-β3. Thus, the safety of blockade of laten TGF-β1 activation may be explained by the fact that the function of TGF-β2 and TGF-β3 are spared. The adverse events observed in an IPF phase IIb randomized

study with an anti-αvβ6 antibody may have been related to the proinflammatory effect of TGFβ inhibition[43]. These results suggest that blockade of integrin αvβ6-mediated latent TGF-β1 activation is associated with long-term safety issues, which also limits the use of latent TGF-β1 blockade as an approach for treating fibrosis. The fact that SOF10 does not affect integrin αvβ6-mediated latent TGF-β1 activation may make it a safer and more effective approach for targeting the TGF-β1 pathway to treat both fibrosis and cancer.

This study has two important limitations. First, although SOF10 has antifibrotic effects in preclinical rodent models, human diseases cannot always be fully recapitulated in rodent models. Fibrosis turnover occurs more slowly in humans than in rodent models. Thus, clinical trials in humans are needed to evaluate the efficacy of SOF10 in the treatment of fibrotic diseases and cancer when combined with ICIs. Second, SOF10 had no adverse effects in the 13-week repeated intravenous dose toxicity (GLP) studies. However, as SOF10 would need to be used for a longer duration in humans, the clinical safety of SOF10 should be further evaluated in the future clinical studies.

In summary, we demonstrate that inhibiting latent TGF-β1 activation by various fibrosis-related proteases and integrin αvβ8 is a safe strategy for treating fibrotic disease and cancer. Fibrosis is a common mechanism underlying all types of organ failure, and our study revealed that SOF10 is a safe and effective therapy for fibrosis in a broad range of organs. Additionally, SOF10 synergizes with ICIs by modulating stromal cells and T cells; therefore, the combination of SOF10 and ICIs is an option for the treatment of cancers strongly associated with fibrosis such as pancreatic cancer. Clinical studies of SOF10 are currently underway for patients with solid cancer (NCT05867121).

Data availability

All data associated with this study are presented in the paper or the Supplementary Materials. The sequences of SOF10 have been published in the patent application (WO 2021/039945)[74]. The structures of SOF10 Fab and latent-TGF-β have been deposited in the RCSB Protein Data Bank under the PDB code 9VJJ. Cif and Pdb file of the structure are provided as Supplementary Data 1 and 2. Source data for Figs. 1, 3, 4, and 5 and Figure S3, S5, S6, and S7 is in Supplementary Data 3.

Received: 2 December 2024; Accepted: 20 January 2026;
Published online: 28 January 2026

References

1. Blobe, G. C., Schiemann, W. P. & Lodish, H. F. Role of transforming growth factor beta in human disease. *N. Engl. J. Med.* **342**, 1350–1358 (2000).
2. Michelotti, G. A., Machado, M. V. & Diehl, A. M. NAFLD, NASH and liver cancer. *Nat. Rev. Gastroenterol. Hepatol.* **10**, 656–665 (2013).
3. Zhou, D. & Liu, Y. Renal fibrosis in 2015: Understanding the mechanisms of kidney fibrosis. *Nat. Rev. Nephrol.* **12**, 68–70 (2016).
4. Piersma, B., Hayward, M. K. & Weaver, V. M. Fibrosis and cancer: A strained relationship. *Biochim Biophys. Acta Rev. Cancer* **1873**, 188356 (2020).
5. Martinez, V. G., Park, D. & Acton, S. E. Immunotherapy: Breaching the barriers for cancer treatment. *Philos. Trans. R. Soc. Lond. B Biol. Sci.* **374**, 20180214 (2019).
6. Chung, S. W., Xie, Y. & Suk, J. S. Overcoming physical stromal barriers to cancer immunotherapy. *Drug Deliv. Transl. Res* **11**, 2430–2447 (2021).
7. Meng, X. M., Nikolic-Paterson, D. J. & Lan, H. Y. TGF-beta: The master regulator of fibrosis. *Nat. Rev. Nephrol.* **12**, 325–338 (2016).
8. Wipff, P. J., Rifkin, D. B., Meister, J. J. & Hinz, B. Myofibroblast contraction activates latent TGF-beta1 from the extracellular matrix. *J. Cell Biol.* **179**, 1311–1323 (2007).
9. Lebrun, J. J. The dual role of TGFbeta in human cancer: from tumor suppression to cancer metastasis. *ISRN Mol. Biol.* **2012**, 381428 (2012).
10. Mariathasan, S. et al. TGFbeta attenuates tumour response to PD-L1 blockade by contributing to exclusion of T cells. *Nature* **554**, 544–548 (2018).
11. Derynck, R., Turley, S. J. & Akhurst, R. J. TGFbeta biology in cancer progression and immunotherapy. *Nat. Rev. Clin. Oncol.* **18**, 9–34 (2021).
12. Pickup, M., Novitskiy, S. & Moses, H. L. The roles of TGFbeta in the tumour microenvironment. *Nat. Rev. Cancer* **13**, 788–799 (2013).
13. Sanjabi, S., Oh, S. A. & Li, M. O. Regulation of the immune response by TGF-beta: from conception to autoimmunity and infection. *Cold Spring Harb. Perspect. Biol.* **9**, a022236 (2017).
14. Anderton, M. J. et al. Induction of heart valve lesions by small-molecule ALK5 inhibitors. *Toxicol. Pathol.* **39**, 916–924 (2011).
15. Stauber, A. J., Credille, K. M., Truex, L. L., Ehlhardt, W. J. & Young, J. K. Nonclinical safety evaluation of a transforming growth factor β receptor i kinase inhibitor in fischer 344 rats and beagle dogs. *J. Clin. Toxicol.* **4**, 1–10 (2014).
16. Mitra, M. S. et al. A potent pan-TGFbeta neutralizing monoclonal antibody elicits cardiovascular toxicity in mice and cynomolgus monkeys. *Toxicol. Sci.* **175**, 24–34 (2020).
17. Lacouture, M. E. et al. Cutaneous keratoacanthomas/squamous cell carcinomas associated with neutralization of transforming growth factor beta by the monoclonal antibody fresolimumab (GC1008). *Cancer Immunol. Immunother.* **64**, 437–446 (2015).
18. Robbrecht, D. et al. Safety and efficacy results from the expansion phase of the first-in-human study evaluating TGFβ inhibitor SAR439459 alone and combined with cemiplimab in adults with advanced solid tumors. *J. Clin. Oncol.* **40**, 2524–2524 (2022).
19. Martin, C. J. et al. Selective inhibition of TGFbeta1 activation overcomes primary resistance to checkpoint blockade therapy by altering tumor immune landscape. *Sci. Transl. Med* **12**, eaay8456 (2020).
20. Yu, L., Border, W. A., Huang, Y. & Noble, N. A. TGF-beta isoforms in renal fibrogenesis. *Kidney Int* **64**, 844–856 (2003).
21. Rowlinson, S. et al. An anti-TGF-β1 specific mAb demonstrates renal efficacy equivalent to a pan neutralizing mAb in the rat anti-Thy1.1 and mouse db/db models. *J. Am. Soc. Nephrol.* **18**, SA–PO329 (2007).
22. Gabriely, G. et al. Targeting latency-associated peptide promotes antitumor immunity. *Sci. Immunol.* **2**, eaaj1738 (2017).
23. Jackson, J. W. et al. An antibody that inhibits TGF-beta1 release from latent extracellular matrix complexes attenuates the progression of renal fibrosis. *Sci. Signal* **17**, eadn6052 (2024).
24. Kulkarni, A. B. et al. Transforming growth factor beta 1 null mutation in mice causes excessive inflammatory response and early death. *Proc. Natl. Acad. Sci. USA* **90**, 770–774 (1993).
25. Yang, Z. et al. Absence of integrin-mediated TGFbeta1 activation in vivo recapitulates the phenotype of TGFbeta1-null mice. *J. Cell Biol.* **176**, 787–793 (2007).
26. Shouse, A. N., LaPorte, K. M. & Malek, T. R. Interleukin-2 signaling in the regulation of T cell biology in autoimmunity and cancer. *Immunity* **57**, 414–428 (2024).
27. David, C. J. & Massague, J. Contextual determinants of TGFbeta action in development, immunity and cancer. *Nat. Rev. Mol. Cell Biol.* **19**, 419–435 (2018).
28. Ahamed, J. et al. In vitro and in vivo evidence for shear-induced activation of latent transforming growth factor-beta1. *Blood* **112**, 3650–3660 (2008).
29. Okuno, M. et al. Prevention of rat hepatic fibrosis by the protease inhibitor, camostat mesilate, via reduced generation of active TGF-beta. *Gastroenterology* **120**, 1784–1800 (2001).
30. Barcellos-Hoff, M. H. & Dix, T. A. Redox-mediated activation of latent transforming growth factor-beta 1. *Mol. Endocrinol.* **10**, 1077–1083 (1996).
31. Jenkins, G. The role of proteases in transforming growth factor-beta activation. *Int J. Biochem Cell Biol.* **40**, 1068–1078 (2008).

32. Shi, M. et al. Latent TGF-beta structure and activation. *Nature* **474**, 343–349 (2011).
33. Wang, R. et al. GARP regulates the bioavailability and activation of TGFb. *eta. Mol. Biol. Cell* **23**, 1129–1139 (2012).
34. Brown, N. F. & Marshall, J. F. Integrin-mediated TGFbeta activation modulates the tumour microenvironment. *Cancers (Basel)* **11**, 1221 (2019).
35. Dong, X., Hudson, N. E., Lu, C. & Springer, T. A. Structural determinants of integrin beta-subunit specificity for latent TGF-beta. *Nat. Struct. Mol. Biol.* **21**, 1091–1096 (2014).
36. Asano, Y., Ihn, H., Jinnin, M., Mimura, Y. & Tamaki, K. Involvement of alphavbeta5 integrin in the establishment of autocrine TGF-beta signaling in dermal fibroblasts derived from localized scleroderma. *J. Invest Dermatol* **126**, 1761–1769 (2006).
37. Asano, Y. et al. Increased expression of integrin αvβ3 contributes to the establishment of autocrine TGF-β signaling in scleroderma fibroblasts1. *J. Immunol.* **175**, 7708–7718 (2005).
38. Liu, S. et al. Expression of integrin beta1 by fibroblasts is required for tissue repair in vivo. *J. Cell Sci.* **123**, 3674–3682 (2010).
39. Aluwihare, P. et al. Mice that lack activity of alphavbeta6- and alphavbeta8-integrins reproduce the abnormalities of Tgfb1- and Tgfb3-null mice. *J. Cell Sci.* **122**, 227–232 (2009).
40. Huang, X. Z. et al. Inactivation of the integrin beta 6 subunit gene reveals a role of epithelial integrins in regulating inflammation in the lung and skin. *J. Cell Biol.* **133**, 921–928 (1996).
41. Koth, L. L. et al. Integrin beta6 mediates phospholipid and collectin homeostasis by activation of latent TGF-beta1. *Am. J. Respir. Cell Mol. Biol.* **37**, 651–659 (2007).
42. Morris, D. G. et al. Loss of integrin alpha(v)beta6-mediated TGF-beta activation causes Mmp12-dependent emphysema. *Nature* **422**, 169–173 (2003).
43. Raghu, G. et al. A phase IIb randomized clinical study of an anti-αvβ6 monoclonal antibody in idiopathic pulmonary fibrosis. *Am. J. Respir. Crit. Care Med.* **206**, 1128–1139 (2022).
44. Maeda, A. et al. Identification of human IgG1 variant with enhanced FcRn binding and without increased binding to rheumatoid factor autoantibody. *MAbs* **9**, 844–853 (2017).
45. Vonrhein, C. et al. Data processing and analysis with the autoPROC toolbox. *Acta Crystallogr D. Biol. Crystallogr* **67**, 293–302 (2011).
46. Kabsch, W. Xds. *Acta Crystallogr D. Biol. Crystallogr* **66**, 125–132 (2010).
47. Evans, P. R. & Murshudov, G. N. How good are my data and what is the resolution? *Acta Crystallogr D. Biol. Crystallogr* **69**, 1204–1214 (2013).
48. Winn, M. D. et al. Overview of the CCP4 suite and current developments. *Acta Crystallogr D. Biol. Crystallogr* **67**, 235–242 (2011).
49. Tickle, I. J. et al. *Staraniso*. Global Phasing Ltd. (2016).
50. McCoy, A. J. et al. Phaser crystallographic software. *J. Appl Crystallogr* **40**, 658–674 (2007).
51. Emsley, P., Lohkamp, B., Scott, W. G. & Cowtan, K. Features and development of Coot. *Acta Crystallogr D. Biol. Crystallogr* **66**, 486–501 (2010).
52. Adams, P. D. et al. PHENIX: a comprehensive python-based system for macromolecular structure solution. *Acta Crystallogr D. Biol. Crystallogr* **66**, 213–221 (2010).
53. Bricogne, G. B. E. et al. *Buster version 2.11.7*. Global Phasing Ltd. (2017).
54. Williams, C. J. et al. MolProbity: more and better reference data for improved all-atom structure validation. *Protein Sci.* **27**, 293–315 (2018).
55. Iida, M. et al. TNF-alpha induces Claudin-1 expression in renal tubules in Alport mice. *PLoS One* **17**, e0265081 (2022).
56. Ding, H., Xu, Y. & Jiang, N. Upregulation of miR-101a suppresses chronic renal fibrosis by regulating KDM3A via blockade of the YAP-TGF-beta-smad signaling pathway. *Mol. Ther. Nucleic Acids* **19**, 1276–1289 (2020).
57. Matsumoto, M. et al. An improved mouse model that rapidly develops fibrosis in non-alcoholic steatohepatitis. *Int J. Exp. Pathol.* **94**, 93–103 (2013).
58. Pamukcuoglu, M. et al. Peripheral and bone marrow CD34(+) cell levels on chronic myeloproliferative disease. *Hematology* **22**, 74–80 (2017).
59. Walton, K. L. et al. Two distinct regions of latency-associated peptide coordinate stability of the latent transforming growth factor-beta1 complex. *J. Biol. Chem.* **285**, 17029–17037 (2010).
60. Ling, H. et al. Therapeutic role of TGF-beta-neutralizing antibody in mouse cyclosporin A nephropathy: morphologic improvement associated with functional preservation. *J. Am. Soc. Nephrol.* **14**, 377–388 (2003).
61. Song, X. et al. Recombinant truncated latency-associated peptide alleviates liver fibrosis in vitro and in vivo via inhibition of TGF-beta/Smad pathway. *Mol. Med* **28**, 80 (2022).
62. Ghafoory, S. et al. Platelet TGF-beta1 deficiency decreases liver fibrosis in a mouse model of liver injury. *Blood Adv.* **2**, 470–480 (2018).
63. Dennler, S. et al. Direct binding of Smad3 and Smad4 to critical TGF beta-inducible elements in the promoter of human plasminogen activator inhibitor-type 1 gene. *EMBO J.* **17**, 3091–3100 (1998).
64. Martinez-Klimova, E., Aparicio-Trejo, O. E., Tapia, E. & Pedraza-Chaverri, J. Unilateral ureteral obstruction as a model to investigate fibrosis-attenuating treatments. *Biomolecules* **9**, 141 (2019).
65. Cosgrove, D. et al. Collagen COL4A3 knockout: A mouse model for autosomal Alport syndrome. *Genes Dev.* **10**, 2981–2992 (1996).
66. Grauel, A. L. et al. TGFbeta-blockade uncovers stromal plasticity in tumors by revealing the existence of a subset of interferon-licensed fibroblasts. *Nat. Commun.* **11**, 6315 (2020).
67. Wynn, T. A. & Ramalingam, T. R. Mechanisms of fibrosis: Therapeutic translation for fibrotic disease. *Nat. Med* **18**, 1028–1040 (2012).
68. Dong, X. et al. Force interacts with macromolecular structure in activation of TGF-beta. *Nature* **542**, 55–59 (2017).
69. Campbell, M. G. et al. Cryo-EM reveals integrin-mediated TGF-beta activation without release from latent TGF-beta. *Cell* **180**, 490–501.e416 (2020).
70. Zhang, X. et al. GARP on hepatic stellate cells is essential for the development of liver fibrosis. *J. Hepatol.* **79**, 1214–1225 (2023).
71. Dufeys, C., Bodart, J., Bertrand, L., Beauloye, C. & Horman, S. Fibroblasts and platelets: a face-to-face dialogue at the heart of cardiac fibrosis. *Am. J. Physiol. Heart Circ. Physiol.* **326**, H655–H669 (2024).
72. Dodagatta-Marri, E. et al. Integrin alphavbeta8 on T cells suppresses anti-tumor immunity in multiple models and is a promising target for tumor immunotherapy. *Cell Rep.* **36**, 109309 (2021).
73. Takasaka, N. et al. Integrin αvβ8-expressing tumor cells evade host immunity by regulating TGF-β activation in immune cells. *JCI Insight* **3**, e122591 (2018).
74. Kanamori, M. Cross-species anti-latent tgf-beta 1 antibodies and methods of use *International Patent Application* WO2021/039945 (2021).

Acknowledgements

We thank A. Sakamoto and T. Tsushima for protein preparation, and Y. Ruike, S. Ishi, and Y. Teranishi for antibody generation or optimization. We also thank D. Kashiwagi, T. Mizuno, S. Yamamoto, K. Ohtake, Y. Tsuboi, S. Usami, S. Matsuo for conducting experiments. We are grateful to T. Kuramochi, Y. Tomii, M. Endo, T. Torizawa, N. Horiba, A. Kato, M. Azuma for advice on the research. We thank all the research assistants at Chugai Pharmaceutical Co. Ltd. and Chugai Pharmabody Research Pte. Ltd. for their excellent experimental assistance.

Author contributions

M.K., I.S., H.K., K.A., K.O., and H.S. wrote the original draft of the manuscript. M.K., I.S., and H.S. conceptualized and formulated the project. M.K., I.S., H.K., K.N., A.M., Y.K., and N.H. performed experiments. M.K., I.S., C.X.K., Y.S[1]., H.K., K.N., K.A., S.W.G., C.L.P., Y.S[2]., M.S.-K., C.K, K.O., coordinated the experiment. T.K., J.N., T.I., and H.S. supervised the work. M.K., I.S., Y.S[1]., H.K., K.N., A.M., K.A., S.W.G., N.H., K.O., T.K., T.I., and H.S. reviewed and edited the manuscript.

Competing interests

M.K., I.S., H.K., K.N, A.M, K.A., Y.S[2]., M.S.-K., C.K., Y.K., N.H., K.O., T.K., T.I., and H.S. are employees of Chugai Pharmaceutical Co. Ltd. (Chugai). Y.S[1]., and S.W.G. are employees of Chugai's subsidiary, Chugai Pharmabody Research Pte. Ltd.(Chugai Pharmabody Research). J.N was employees of Chugai, and C.X.K and C.L.P. were employees of Chugai Pharmabody Research at the time of the study. H.S. was a Chief Executive Officer of Chugai Pharmabody Research Pte. Ltd. M.K., I.S., H.K., K.N., A.M., K.A., Y.S[2]., M.S.-K., C.K., Y.K., N.H., K.O., J.N., T.K., T.I., and H.S. have stock in Chugai. Chugai has filed patent applications related to the anti-latent TGF-β1 antibodies. M.K. is the inventor of the following patent: CROSS-SPECIES ANTI-LATENT TGF-BETA 1 ANTIBODIES AND METHODS OF USE (WO2019/163927). M.K., H.S., and C.X.K. are the inventors of the following patent: CROSS-SPECIES ANTI-LATENT TGF-BETA 1 ANTIBODIES AND METHODS OF USE (WO2021/039945) and USES OF CROSS-SPECIES ANTI-LATENT TGF-BETA 1 ANTIBODIES (WO2022/180764).

Additional information

Supplementary information The online version contains supplementary material available at https://doi.org/10.1038/s43856-026-01408-w.

Correspondence and requests for materials should be addressed to Hideaki Shimada.

Peer review information *Communications Medicine* thanks Christian Klein, Ruchi Bansal and the other, anonymous, reviewer(s) for their contribution to the peer review of this work.